(12) INTERNATIONAL APPLICATION PUBLISHED UNDER THE PATENT COOPERATION TREATY (PCT)

(19) World Intellectual Property Organization
International Bureau

(43) International Publication Date
29 March 2007 (29.03.2007)

PCT

(10) International Publication Number
WO 2007/033433 A1

(51) International Patent Classification:
G02B 5/30 (2006.01) *H04J 14/06* (2006.01)
G01J 5/58 (2006.01)

(21) International Application Number:
PCT/AU2006/001397

(22) International Filing Date:
25 September 2006 (25.09.2006)

(25) Filing Language: English

(26) Publication Language: English

(30) Priority Data:
2005905262 23 September 2005 (23.09.2005) AU

(71) Applicant *(for all designated States except US)*: **THE AUSTRALIAN NATIONAL UNIVERSITY** [AU/AU]; Acton, Canberra, ACT 0200 (AU).

(72) Inventor; and
(75) Inventor/Applicant *(for US only)*: **HOWARD, John** [AU/AU]; 20 Illingworth Street, Wanniassa, ACT 2903 (AU).

(74) Agent: **SPRUSON & FERGUSON**; G.P.O. Box 3898, Sydney, NSW 2001 (AU).

(81) Designated States *(unless otherwise indicated, for every kind of national protection available)*: AE, AG, AL, AM, AT, AU, AZ, BA, BB, BG, BR, BW, BY, BZ, CA, CH, CN, CO, CR, CU, CZ, DE, DK, DM, DZ, EC, EE, EG, ES, FI, GB, GD, GE, GH, GM, HN, HR, HU, ID, IL, IN, IS, JP, KE, KG, KM, KN, KP, KR, KZ, LA, LC, LK, LR, LS, LT, LU, LV, LY, MA, MD, MG, MK, MN, MW, MX, MY, MZ, NA, NG, NI, NO, NZ, OM, PG, PH, PL, PT, RO, RS, RU, SC, SD, SE, SG, SK, SL, SM, SV, SY, TJ, TM, TN, TR, TT, TZ, UA, UG, US, UZ, VC, VN, ZA, ZM, ZW.

(84) Designated States *(unless otherwise indicated, for every kind of regional protection available)*: ARIPO (BW, GH, GM, KE, LS, MW, MZ, NA, SD, SL, SZ, TZ, UG, ZM, ZW), Eurasian (AM, AZ, BY, KG, KZ, MD, RU, TJ, TM), European (AT, BE, BG, CH, CY, CZ, DE, DK, EE, ES, FI, FR, GB, GR, HU, IE, IS, IT, LT, LU, LV, MC, NL, PL, PT, RO, SE, SI, SK, TR), OAPI (BF, BJ, CF, CG, CI, CM, GA, GN, GQ, GW, ML, MR, NE, SN, TD, TG).

Published:
— *with international search report*

For two-letter codes and other abbreviations, refer to the "Guidance Notes on Codes and Abbreviations" appearing at the beginning of each regular issue of the PCT Gazette.

(54) **Title:** MULTI-COHERENCE IMAGING SYSTEM AND METHOD

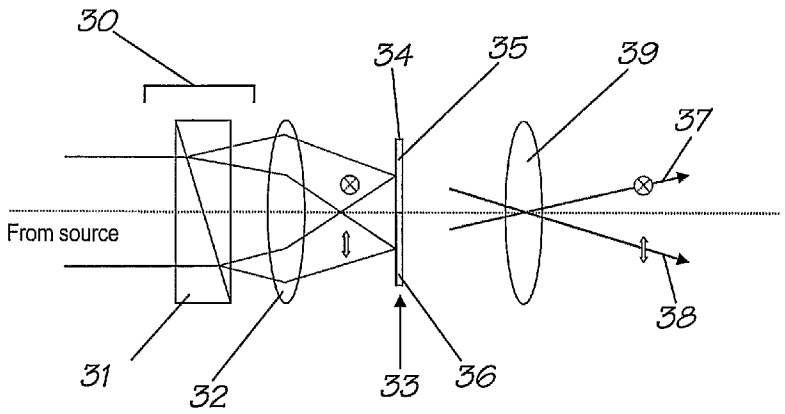

(57) **Abstract:** The present invention relates to imaging and in particular to multi-spectral imaging which relies on sampling the time-domain optical coherence at appropriately chosen set of delays. The invention has been developed primarily for use as a multi-coherence imaging system and arrangements of the invention comprise a polarizing image mask for providing angularly multiplexed, dual orthogonal polarized beams, each beam being a replica of an incoming radiation beam from a source, the polarising image mask comprising a first Wollaston prism as a first polarizing component for providing angularly multiplexed radiation beams from the incoming radiation beam, the beams being multiplexed in a first direction; and a split field polarizer comprising adjoining, orthogonally oriented polarizing materials for providing angularly multiplexed, dual orthogonal polarized radiation beams.

WO 2007/033433 A1

MULTI-COHERENCE IMAGING SYSTEM AND METHOD

TECHNICAL FIELD

[0001] The present invention relates to imaging and in particular to multi-spectral imaging which relies on sampling the time-domain optical coherence at appropriately chosen set of delays T_k. The invention has been developed primarily for use as a multi-coherence imaging system and will be described hereinafter with reference to this application. However, it will be appreciated that the invention is not limited to this particular field of use.

BACKGROUND OF THE INVENTION

[0002] Any discussion of the prior art throughout the specification should in no way be considered as an admission that such prior art is widely known or forms part of the common general knowledge in the field.

[0003] Recent advances in computing power and detector technology have seen growth in the development of multi-colour imaging systems for wide array of diagnostic applications in research, industry and defence. Some of the applications for these so-called "multi-spectral" and "hyper-spectral" imaging systems include geological, oceanographic and agricultural remote sensing, remote inspection of foodstuffs (fruit, poultry), detecting/characterizing human skin lesions, thermal imaging, and scientific applications in astronomy, plasma physics and combustion research. Almost all of the current technologies use space and/or time multiplex techniques to sample and acquire the ``data cube" that represents the discretized image scene (x_i, y_j) in multiple colours λ_k.

Multi-Spectral Imaging

[0004] There are a great many approaches to sampling and processing the spectral data cube. The use of multiple cameras is expensive and suffers problems due to parallax and image registration. Low colour-resolution systems can multiplex the colour information through a common aperture camera by using focal plane detectors comprised of stacked or interleaved arrays of detecting elements having complementary regions of spectral sensitivity. Alternatively, using a combination of prisms and filters, the colour scene can be spatially multiplexed onto different regions of a detector array. These systems tend to be optically complex, and can suffer from reduced dynamic range by having to simultaneously accommodate regions of different spectral intensity.

[0005] A tunable colour-selecting device such as a rotatable colour filter array multiplexes the colour information in the time domain by utilizing successive image frames to record information in different

bands. These systems are mechanically cumbersome and slow. Alternatively, electronically tunable acousto-optic cells [1] or liquid-crystal tunable Lyot birefringent filter systems can be used as the colour selecting element. The latter system, which is commercially available (VariSpec, www.cri-inc.com) is slow to tune (of the order of about 100ms), suffers vignetting, and low throughput (typically 15%) because of the nature of the tunable birefringent filter.

[0006] Another approach is to spatially scan the scene using an instrument that disperses the spectrum in one direction of the detector array and views a slit section of the scene in the other [2]. The hybrid chromo-tomographic approach uses a dispersing prism to produce a spatial-spectral projection of the data cube. By rotating the cube and generating successive image frames it is possible to use tomographic techniques to restore the data-cube [3]. This time-multiplex method has high throughput but suffers the usual noise amplification problems associated with poorly conditioned inverse methods.

[0007] Fourier transform spectrometers (interferometers) offer some potential advantages over slit-coupled rating spectrometers, including higher light throughput [4] and the ability to obtain two dimensional mages. These advantages have not previously been fully exploited or multi-spectral imaging applications because of the perceived need to scan the interferometric optical path length delay in order o measure the spectral coherence, and the difficulty of constructing stable optical interferometers with a wide field-of-view.

[0008] The signals at the output ports of a dual beam interferometer are related to the complex coherence of the light source radiation:

$$S_{\pm}(\tau) = (I_0/2)[\,1 \pm \Re(\gamma(\tau))\,] \qquad (1)$$

[0009] Here I_0 is the spectrally integrated emission intensity, τ is the optical path time delay between interfering wavefronts and $\gamma(\tau)$ is the optical coherence, related to the light spectral radiance $H_\nu(\nu)$ through the Weiner-Khinchine theorem

$$\gamma(t) = (1/I_0)\int H_\nu(\nu)\exp(i2\pi\nu\tau)d\nu \qquad (2)$$

[0010] For the special case of quasi-monochromatic radiation having mean optical frequency ν_0 the interferometer signals can be written as

$$S_{\pm}(\tau) = (I_0/2)[\,1 \pm \varsigma\cos(2\pi\nu_0\tau)\,] \qquad (3)$$

where the fringe contrast ζ is determined by the spectral distribution around ν_0 and the interferometric phase depends on the mean frequency and the optical delay. Thus, a shift in spectral centre-of-mass ν_0, appears as a change in the optical phase, with a corresponding change in the interferometer light intensity.

[0011] Instruments which exploit some of these advantages are the compact, static Fourier-transform spectrometers developed by Padgett and others [5]. These devices produce an image of the interferogram

along one axis of the detector array and a spatial line-scan in the other. They have the advantage of high light throughput and are well suited for 1-d imaging applications. These systems can produce 2-d images only through the accumulation of a sufficient number of line scans obtained by slit-scanning the object image.

[0012] In the past few years, the present applicant has developed electro-optically modulated polarization interferometers for wide-field time-resolved "coherence-imaging", with applications in plasma Doppler spectroscopy [6], polarization spectroscopy [7] and infrared thermography [8], the contents of which are wholly incorporated herein by cross-reference. After isolating the spectral region of interest using an interference filter, it is possible to use one or more electro-optically modulatable birefringent plates placed between a polarizer and analyser to encode the spectral information over a spread of harmonics of the modulation frequency [9], the contents of which are wholly incorporated herein by cross-reference.

[0013] For a simple polarization interferometer, a single fixed-delay waveplate is placed with its fast axis at 45 degrees to the orientation of a first polarizer and final analyzer. The plate mutually delays the polarization components parallel and perpendicular to the fast axis. If the waveplate is also electro-optic, the application of a high voltage along an appropriate crystal axis of the waveplate will allow the optical path delay to be modulated in order to measure the local fringe properties as shown in **Figure 1**. In conjunction with field-of-view widening techniques, suitable imaging optics and 2-d detector arrays – such as fast-framing charge-coupled device detectors (CCDs) or multi-anode photo-multiplier tube detectors (PMTs) – it is possible to perform time-resolved 2-d imaging of the complex coherence of the spectral scene.

[0014] A drawback of the simple polarization interferometer, however, is that half of the incident light is discarded by the first polarizer, thereby greatly reducing the available signal reaching the detector array for analysis.

[0015] A generalization of the modulated single delay spectrometer suitable for the study of quasi-monochromatic spectral scenes, that utilizes a number of birefringent electro-optic plates mutually aligned at 45° has been reported in [9]. The so-called Spread-spectrum Optical Fourier Transform (SOFT) spectrometer allows simultaneous measurements of the coherence at a multiplicity of delays. As the name suggests, the information is encoded over a series of harmonics of a common sinusoidal drive voltage applied to the electro-optic crystals.

[0016] A typical 3-crystal layout for the SOFT spectrometer is shown in **Figure 2**. The birefringent crystals (having N = 3 different delays ϕ_1, ϕ_2 and ϕ_3) are mutually oriented at 45 degrees and placed between parallel or crossed polarizers to give rise to give a number of independent fixed delay interferometers. The optical layout is reminiscent of a Solc birefringent filter in which the tilt angles of an assembly of identical birefringent plates can be adjusted to produce a tunable narrowband interference filter [11,12]

[0017] For example, a system consisting of N = 3 crystals having delays $\phi_1 = \phi_0$, $\phi_2 = 3\phi_0$, $\phi_3 = 5\phi_0$ gives six independent interferometers having fixed delays $\{|\phi_1 \pm \phi_3|, |\phi_1 \pm \phi_2 \pm \phi_3|\} = \{1,3,4,6,7,9\}\phi_0$. The signal at the interferometer output ports is given by

$$S_{\pm}(\tau) = (I_0/2)[1 \pm \sum_i w_i \gamma(\tau_i)] \qquad (4)$$

where the sum is over the set of six independent delays τ_i and the weights w_i depend on the relative orientation of the birefringent plates. For quasi-monochromatic radiation, the signal can be expressed as

$$S_{\pm}(\tau) = (I_0/2)[1 \pm \sum_i w_i \varsigma_i \cos\phi_i] \qquad (5)$$

where the ζ_i are the local fringe visibilities at optical phase delays ϕ_i that depend on the mean spectral wavelength and the set of optical delays τ_i.

[0018] The degeneracy among the different delay components can be broken by applying the same sinusoidal modulating voltage to each of the birefringent plates. The resulting modulation indices are in the same ratio as the various delays. The larger the delay, the greater is the modulation depth and the higher in frequency are the associated harmonic carriers. The spectral information can then be extracted numerically or electronically using a series of bandpass filters centred on the respective carriers and having a maximum bandwidth determined by the modulation frequency. Inverse FFT recovers a set of time vectors that can be unwrapped with good condition to extract 12 independent pieces of information pertaining to the temporal evolution of the spectral scene.

[0019] Some drawbacks of this approach are that the light is shared among a number of harmonics simultaneously, ultimately compromising the signal to noise ratio. In addition, to maximize the available signal bandwidth and simplify the demodulation procedure, the plate thicknesses must share a common divisor (this condition is relaxed below). The continuous sinusoidal modulation strategy is suitable only for the interpretation of quasi-monochromatic scenes, and is not well adpated to imaging using fast digital cameras. At a practical level, the electro-optic plates need to be biased at high voltage (~ kV) to achieve the desired modulation index.

[0020] The term "comprising" as used herein means "including principally, but not necessarily solely". Furthermore, variations of the word "comprising", such as "comprise" and "comprises", have correspondingly varied meanings.

SUMMARY OF THE INVENTION

[0021] It is an object of the present invention to substantially overcome or at least ameliorate one or more of the above disadvantages, or to provide a useful alternative.

[0022] In a first aspect this invention provides a polarizing image mask for providing angularly multiplexed, dual orthogonal polarized beams, each beam being a replica of an incoming radiation beam from a source. The polarizing mask may comprise a first Wollaston prism as a first polarizing component for providing angularly multiplexed radiation beams from the incoming radiation beam, the beams being multiplexed in a first direction. The polarizing mask may further comprise a split field polarizer. The split-field polariser may comprise adjoining, orthogonally oriented polarizing materials for providing angularly multiplexed, dual orthogonal polarized radiation beams.

[0023] The polarizing image mask for providing angularly multiplexed, dual orthogonal polarized beams, each beam being a replica of an incoming radiation beam from a source, the polarising image mask comprising: a first Wollaston prism as a first polarizing component for providing angularly multiplexed radiation beams from the incoming radiation beam, the beams being multiplexed in a first direction; and a split field polarizer comprising adjoining, orthogonally oriented polarizing materials for providing angularly multiplexed, dual orthogonal polarized radiation beams.

[0024] The polarizing mask produces dual orthogonal polarized, replicas of a source image that are angularly multiplexed. The split-field-polarizer may consist of adjoining, orthogonally oriented polarizing materials. The Wollaston prism may be placed in front of an objective lens to produce dual, orthogonally polarized images in the lens image plane. The split-field-polarizer may be located in the image plane so as to transmit and isolate the orthogonally polarized images.

[0025] It will be apparent that the separated orthogonally polarized images act as independent anti-phase, angularly multiplexed sources. The orthogonally polarized images may then be passed through subsequent polarization interferometer optics which effectively act as independent interferometers.

[0026] The polarizing image mask may further comprise an optical power element thereby to produce dual, orthogonally polarized images in the image plane of the optical power element.

[0027] The split-field-polarizer may be located in the image plane of the optical power element thereby to isolate the orthogonally polarized images. The split-field-polarizer may be fabricated using standard deposition techniques and custom manufactured in accordance with requirements.

[0028] The angularly multiplexed orthogonally polarized radiation beams may be passed through respective polarization interferometer optics. The angularly multiplexed orthogonal polarization images may be independently manipulated at the polarized image mask in accordance with requirements.

[0029] The polarizing image mask may further comprise at least one colour filter to isolate a spectral region of interest.

[0030] The polarizing image mask may further comprise a quarter wave plate inserted in one of the orthogonally polarized images at the polarization mask thereby to introduce a 90 degree relative phase shift between the orthogonally polarized images. When combined with a fixed delay wave plate and a final splitting Wollaston prism a quadrature sampling of the interferogram may be achieved. That is, the

resulting four-quadrature image may provide a snap shot of the local interferogram phase and contrast without temporal multiplexing. This facilitates very fast imaging of simple Doppler spectral scenes using, for example, a framing streak camera.

[0031] The polarizing image mask may further comprise a second Wollaston prism aligned substantially orthogonal to the first Wollaston prism for further angularly multiplexing the angularly multiplexed orthogonal polarization radiation beams in a second direction. The second direction is substantially orthogonal to the first direction.

[0032] According to a second aspect of the invention, there is provided an image forming system capable of acting upon an incoming radiation beam from a source. The system may comprise a polarization mask comprising a first Wollaston prism as a first polarizing component. The system may further comprise a split field polarizer. The split-field polariser may comprise comprising adjoining, orthogonally oriented polarizing materials. The polarisation mask may produce dual orthogonal polarized beams which are angularly multiplexed in a first direction.

[0033] The system may further comprise a polarization element for providing images of each of the dual angularly multiplexed orthogonal polarized on an imaging detector array.

[0034] The system may further comprise an electro-optical delay switch for switching the optical path delay in accordance with requirements. The system may further comprise further comprising a collimating optical power element for collimating the angularly multiplexed dual orthogonal polarized beams. The delay switch may be formed from a ferroelectric liquid crystal compound.

[0035] The imaging detector array may have an image frame rate, and the delay switch may be synchronised with the detector array frame rate. The imaging detector array may be selected from a charge coupled device camera or a framing streak camera or other multi-element detector device.

[0036] The polarization element may comprise a second Wollaston prism aligned substantially orthogonal to the first Wollaston prism for further angularly multiplexing the angularly multiplexed orthogonal polarization radiation beams in a second direction.

[0037] The system may further comprise at least one filter for providing a coherence image of desired spectral content to be imaged on the detector array. The system may further comprise a plurality of filters, each filter transmitting an independent spectral pass bands for providing coherence images of distinct spectral content to be imaged on the detector array. The filters may be selected from dichroic or interference filters. The filter may be incorporated into the polarization mask.

[0038] The system may further comprise a polarization stage and imaging optical power element to image each of the angularly multiplexed information into spatial distinct images on the detector array. The polarization stage may be selected from a simple polarizer, a Wollaston prism, or a further polarization mask.

[0039] According to a third aspect of the invention, there is provided a spatio-temporal multiplex optical system comprising:

a polarizing image mask comprising: a first Wollaston prism for providing angularly multiplexed radiation beams from the incoming radiation beam, the beams being multiplexed in a first direction; and a split field polarizer comprising adjoining, orthogonally oriented polarizing elements for providing angularly multiplexed, dual orthogonal polarized radiation beams;

a collimating optical power element;

an optical delay switch for modifying the polarization of the angularly multiplexed, dual orthogonal polarized radiation beams;

a second Wollaston prism for providing further angularly multiplexed radiation beams from the angularly multiplexed, dual orthogonal polarized radiation beams, the beams being further angularly multiplexed in a second direction;

a detector array for receiving each of the four angularly multiplexed radiation beams; and

an imaging optical power element for focusing the four angularly multiplexed radiation beams to respective substantially spatially distinct region of the detector array.

[0040] The hybrid arrangement may have application for more complex, narrow or broadband scenes that require more than three parameter fields for their description.

[0041] According to a fourth aspect of this invention there is provided a method for providing angularly multiplexed, dual orthogonal polarized beams, each beam being a replica of an incoming radiation beam from a source, the method comprising:

providing angularly multiplexed radiation beams from the incoming radiation beam, with a first polarizing component, the beams being multiplexed in a first direction; and

providing angularly multiplexed, dual orthogonal polarized radiation beams with a split field polarizer comprising adjoining, orthogonally oriented polarizing materials.

[0042] The fist polarizing component may be a Wollaston prism.

[0043] The method may further comprise the step of introducing a 90 degree relative phase shift between the orthogonally polarized images.

[0044] The method may further comprise the step of angularly multiplexing the orthogonal polarization radiation beams in a second direction.

[0045] The method may further comprise imaging at least two angularly multiplexed radiation beams or four angularly multiplexed radiation beams onto spatially distinct regions on a detector.

[0046] The method may further comprise outputting signal from each of the spatially distinct regions on the detector and comparing the signals. At least one of the temperature, brightness or flow speed of an object or fuid or plasme may be determined from the comparing of the signals.

BRIEF DESCRIPTION OF THE DRAWINGS

[0047] A preferred embodiment of the present invention will now be described, by way of an example only, with reference to the accompanying drawings wherein:

[0048] **Figure 1** is a three dimensional perspective view of an optical arrangement for the simple modulated fixed delay of the prior art;

[0049] **Figure 2** is a three dimensional perspective view of the relative orientation of the polarizers and birefringent crystals for a 3-crystal SOFT spectrometer of the prior art;

[0050] **Figure 3** is a schematic plan representation of an optical arrangement for producing angularly separated, orthogonally polarized, independent image sources for hybrid coherence imaging system;

[0051] **Figure 4** is a three dimensional schematic view of an optical arrangement for a split-image coherence-phase imaging system of **Figure 3**;

[0052] **Figure 5** is a depiction of the fast axis switching of a ferroelectric liquid crystal (FLC) and the relative alignment of FLC and waveplate axes in FLC "off" and "on" states;

[0053] **Figure 6A** graph of the variation of universal blackbody spectrum and the radiometric temperature sensitivity factor as a function of dimensionless parameter x;

[0054] **Figure 6B** is a graph of the contours of the parameter x versus radiation wavelength and source temperature.

[0055] **Figure 7A** is a graph depicting the variation of blackbody spectrum as a function of temperature in the range 1500K to 1900K (typical molten iron temperatures);

[0056] **Figure 7B** is a graph depicting the variation of the computed interferogram of light passed by the ideal rectangular filter centred on 900nm (at left) as a function of optical delay (MgF2 birefringent plate thickness) and for temperatures in the range 1500K to 1900K;

[0057] **Figure 8** is a graph of interferometric intensity versus phase delay offset which illustrates the operating principle for measuring coherence phase;

[0058] **Figure 9** is a schematic representation of an optical arrangement for simple split-image coherence-phase imaging system;

[0059] **Figure 10** is a three dimensional schematic view of an optical arrangement for a split-image coherence-phase imaging system of **Figure 6**;

[0060] **Figure 11** shows split images of a molten iron stream which may be processed in accordance with the invention to retrieve iron temperature and emissivity;

[0061] **Figure 12** is a graph of ideal brightness (ε=1) and coherence temperature versus frame number (top) averaged over the region shown in Fig. 9 for a sequence of such images and the inferred emissivity of the region (bottom); and

[0062] **Figures 13A and 13B** are respectively elevation and plan views of an optical arrangement for producing 4-quadrant, quadrature-multiplexed coherence image of a thermal source;

[0063] **Figure 14** is a schematic diagram showing the definition of the various symbols used in the analysis of the pyrometry signal processing algorithm;

[0064] **Figure 15** is a false colour 4-quadrant image of a scalpe blade seen against an interference pattern produced with the arrangement of **Figure 13A**;

[0065] **Figure 16** is a typical contrast image from 4 quadrant system using field-widened delay plates (2 x 15mm lithium niobate);

[0066] **Figure 17** is a contour plot of the sine of the phase difference between the upper and lower calibration image pairs showing a high degree of quadrature across most of the image area.

[0067] **Figures 18A** and **18B** are respectively a schematic view of a plasma viewing arrangement and an AUTOCAD model of the camera view through the vacuum port window of the viewing arrangement in the absence of a plasma.

[0068] **Figure 19** is a raw 4-quadrant 512x512 image (where the individual images are inverted) of a plasma pulse in the arrangement of **Figures 18A** and **18B** with an exposure time of 50 ms; and

[0069] **Figure 20** is a contour plot of a reduced 4 quadrant image showing average brightness, ion temperature and flow fields for the 4-quadrant image of **Figure 19**.

DETAILED DESCRIPTION OF THE PREFERRED EMBODIMENTS

[0070] When the spectral content of a scene can be adequately described by a small number of free parameters (e.g. Doppler broadening, blackbody radiation, polarized multiplets), it is often the case that these parameters can be recovered from measurements of the complex coherence at a small number of appropriately chosen fixed optical path length delays. The complex coherence, which is the time-domain equivalent (Fourier transform) of the colour spectrum, can be measured using interferometric techniques. For example, changes in the spectral centre-of-mass (colour balance) in a given passband will give rise to an easily measurable change in the interferometric phase. Throughout this document, this alternative approach is referred to as "multi-coherence" imaging.

[0071] An electro-optically modulated, fixed-delay imaging interferometer for high resolution spectroscopy of quasi-monochromatic spectral scenes has been previously described in [9,6], the contents of which are wholly incorporated herein by cross-reference. In that method, the spectral information is encoded at multiple harmonics of the modulation frequency.

[0072] In the present system, a hybrid imaging approach where antiphase coherence images at one or more delays are multiplexed spatially into separate regions of the detector array is presented, where the coherence is sampled at multiple optical delay offsets synchronously with the image acquisition rate. The temporal sampling is achieved using compound elements constructed of switchable ferroelectric liquid crystal waveplates combined with fixed delay waveplates. The spatial multiplexing is achieved using polarization based components which allow a compact, high throughput optical design.

Hybrid coherence imaging system

[0073] As previously mentioned, a drawback of the simple polarization interferometer of the prior art is that half of the incident radiation is discarded by the first polarizer. It is possible to utilize this otherwise wasted component by using a Wollaston prism as the first polarizing component and thereafter angularly multiplexing the orthogonally polarized images through separate, effectively independent, interferometers.

[0074] Disclosed herein is a new approach based on the use of polarizing optical components to produced spatially multiplexed, independent images of the complex coherence in two halves, or four quadrants of an imaging detection system (e.g. a CCD camera).

[0075] To characterize more complex spectral scenes, it is necessary to obtain additional information. With the introduction of compound switchable ferroelectric liquid crystal (FLC)/delay-plate combinations, it becomes possible to image different regions of the interferogram synchronously with the camera frame rate.

[0076] Arrangements of the present system may be functionally separated into three units:

a) **Polarizing image mask - angular/spatial multiplex:** This module includes a method for producing dual, orthogonally polarized, replicas of the source image that are angularly multiplexed through the remaining interferometer optics. The polarization image mask can incorporate one or more colour filters which isolate the spectral region(s) of interest. The polarization states of the dual images can also be independently manipulated at the mask.

b) **Switching optical delay - temporal multiplex:** These optics are used to introduce fixed or switchable birefringent optical path delays which are essentially common to both sources. Described herein is temporal multiplexing optical arrangements and a method for switching the optical path delay over a range of values in synchronism with the frame

rate of an imaging detector array such as a CCD camera. A collimating lens can be used to match this unit with the initial mask. For wide field-of-view applications, the angular dependence of the birefringent plate phase delay can be almost completely eliminated using standard field-widening techniques [10].

c) **The image forming system:** This consists of a final polarization stage and lens to convert the angularly multiplexed information into spatially distinct images on the detector array. The polarization stage can be a simple polarizer, a Wollaston polarizing prism or a polarization mask as in (a).

[0077] The optical properties of functional units (a) and (b) are described in further detail below before indicating how the units can be combined for particular spectroscopic applications (both high and low resolution) where a coherence imaging approach opens previously inaccessible avenues of study.

[0078] The example arrangements of the system disclosed herein include a static split-frame fixed-delay polarization interferometer for colour-balance discrimination. Such systems can be used in broadband ($\lambda/\Delta\lambda$ ~10) spectral applications, such as coherence pyrometry, or near-infrared reflectance spectroscopy, which often arise in industrial or remote sensing contexts.

[0079] The split-frame arrangement can be generalized for 4-quadrant coherence imaging with applications in high speed, high-resolution ($\lambda/\Delta\lambda$ > 100) Doppler spectroscopic imaging studies of combustion systems, inertial plasma confinement, shock tubes, fusion plasmas etc.

[0080] For more complex, narrow or broadband scenes that require more than three parameter fields for their description, hybrid spatio-temporal multiplex optical arrangements may be employed based on switching FLC/delay-plate compound components combined with a static split or quad-frame optical layout and such arrangements are discussed further below.

Polarization masking

[0081] As shown in **Figure 3**, a polarisation mask **30**, such as a Wollaston prism **31**, is placed in front of objective lens **32** to produce dual, orthogonally polarized images in the lens image plane **33**. A split-field-polarizer **34** consisting of adjoining, orthogonally oriented polarizing materials **35** and **36** is located in the image plane **33** so as to transmit and isolate the orthogonally polarized images. The split-field-polarizer **34** is fabricated using standard deposition techniques and may be custom manufactured to specification as required. The separated, orthogonally polarized images **37** and **38** act as independent, anti-phase, angularly multiplexed sources for the subsequent polarization interferometer optics, which are collimated by collimating lens **39**..

[0082] Depending on the application, additional optical components may be introduced at the polarization mask **30**. For example, for plasma Doppler spectroscopy applications, a quarter wave plate inserted in one of the images at the first polarization mask introduces a 90° relative phase shift between

the independent sources. When combined with a common fixed delay waveplate and a final splitting Wollaston, the system delivers a quadrature sampling of the interferogram. In other words, the resulting 4-quadrant image gives a snapshot of the local interferogram phase and contrast without recourse to temporal multiplexing. It is therefore facilitates very fast imaging of simple Doppler spectral scenes using, for example, a framing streak camera, a capability that has not previously been realised.

[0083] Common or independent spectral passbands can also be selected using one or more dichroic or interference filters located at the split-field-polarizer mask. Independent coherence images of the distinct colour scenes can then be produced at the detector.

Multiple delay systems and optical delay modulation strategies

[0084] For the electro-optically modulated polarization interferometer, the optical phase delay changes in proportion to the amplitude of the externally applied electric field, with the optical axis direction remaining approximately fixed. On the other hand, ferroelectric liquid crystals (FLCs) are optically equivalent to a linear waveplate of fixed delay, but whose optical axis can be switched through a prescribed angle (typically 45°) depending on the polarity of an applied DC voltage. Disclosed hereunder are phase-step modulation methods based on both approaches.

Electro-optical delay stepping

[0085] For fast digital two dimensional imaging using a framing camera, the coherence information is retrieved by stepping the optical phase in synchronism with the camera frame rate. For quasi-monochromatic scenes, the number of required phase steps is equal to 2N + 1 where 2N corresponds to the two quadrature components per delay plus the unknown intensity I_0. The latter can be determined by imaging both bright and dark fringe patterns simultaneously using a final splitting Wollaston prism and taking the average of the images. For example, the signals from a dual-plate interferometer constructed using waveplates mutually oriented at 45° between polarizers oriented also at 45° are given by

$$S_{\pm}(\tau) = (I_0/2)\left[1 \pm \frac{1}{2}\varsigma_{1+2}\cos(\phi_1+\phi_2) \mp \frac{1}{2}\varsigma_{1-2}\cos(\phi_1-\phi_2)\right] \qquad (6)$$

[0086] Denoting the applied phase step on the dual-plate combination as (δ_1, δ_2), it is straightforward to show that the modulation sequence (0,0), (0, $\pi/2$), ($\pi/2$, 0), ($\pi/2$, $\pi/2$) will deliver the quadrature components of the optical coherence at delays $\phi_1 \pm \phi_2$. This approach is suitable for relatively narrowband scenes, where the variation of the coherence phase is approximately linear in the vicinity of the delay offset so that the local interferometric phase and contrast can be determined from quadrature measurements.

[0087] For a triple-birefringent-plate system, a total of six independent interferometers having delays $\{|\phi_1+/-\phi_3|, |\phi_1+/-\phi_2+/-\phi_3|\}$ are formed, so that twelve independent images may be generated by phase-stepping.

FLC polarization switching

[0088] Half-wave delay FLCs are widely used as optical shutters in which the FLC is sandwiched between co-aligned polarizers and oriented so as to transmit incident polarized light (fast optical axis parallel to the polarizer axis) in its "off" state. When the polarity of the applied dc voltage is reversed (about ±10V), the waveplate axis switches rapidly (about 10 μs or less) through 45° so as to act as a half-wave plate, rotating the incident polarization direction such that the light is blocked by the final polarizer. This situation is depicted in **Figure 5** where the "off" state is designated "FLC state 0" **50** and the "on" state where the waveplate axis is rotated through 45° is designated as "FLC state 1" **55**.

[0089] Switchable waveplates can be combined with birefringent plates to allow the construction of a rich array of variable optical delay interferometers. Reference to the FLC axis in the discussion of the following arrangements refers to the direction of the fast axis in the "off" state as shown in **Figure 5**.

[0090] By way of example, consider a compound element consisting of a fixed delay waveplate and FLC whose fast axes are parallel. Let the waveplate and FLC plate have delays (τ,δ) respectively. When sandwiched between parallel polarizers and oriented with fast axis at 45° to the polarizer axes, the "off"-state **50** system acts as an interferometer of total delay $\tau + \delta$. When the FLC switches orientation (to the "on"-state **55**), its axis is parallel to the first polarizer and the total delay τ is that due to the waveplate alone. Such a system is therefore another form of modulated polarization interferometer whose delay can be varied in step-like fashion by δ but without the need for high voltages.

[0091] For narrowband scenes, and if δ is chosen to be a quarter wave, the compound element when used in conjunction with a final Wollaston can be used to generate spatio-temporal multiplexed quadrature images of the fringe coherence near the fixed delay offset τ. It follows that using a combination of switchable compound plates, it is possible to recover fringe contrast and phase at a number of independent optical delays determined by the set of delay plate thicknesses. For example, consider a system composed of three compound FLC-waveplate components between polarizers. Three plates produce 12 independent delays, while the switching FLCs allow access only to $2^3 = 8$ independent frames. In this case, the degeneracy can be removed by inserting a fourth switchable FLC plate.

Split image System – Coherence Pyrometry

[0092] When the temperature of a body increases, the primary colour of the light that it radiates shifts towards the blue. For example, as a simple filament heats up, its colour changes from dull red through to

brilliant white. The radiated power also increases dramatically. Either the colour change (colour pyrometry) or the absolute radiated power (radiometry) can be used to estimate the temperature of the body in question i.e. the filament. Radiometric thermal imaging systems rely on assumed knowledge of the radiant efficiency (emissivity) of hot targets. This is a source of error and can compromise reliability in some applications.

[0093] The blackbody spectrum at temperature T can be expressed in the form

$$H_\nu(\nu;T) = \frac{aT^3x^3}{\exp(x)-1}$$

where $x = hc/\lambda kT$ is a dimensionless "blackbody parameter". If the source temperature increases incrementally by δT the radiant intensity also increases such that

$$\frac{\delta H_\nu}{H_\nu} = \rho(x)\frac{\delta T}{T}$$

where

$$\rho(x) = \frac{x\exp(x)}{\exp(x)-1}$$

[0094] is the normalized differential radiometric temperature sensitivity. **Figures 6A** and **6B** respectively show the variation of universal blackbody spectrum and the radiometric temperature sensitivity factor as a function of dimensionless parameter; and the parameter x versus radiation wavelength and source temperature. Note from **Figure 6B** that $\rho(x) \approx x$ is an excellent approximation over much of the spectrum.

[0095] If the emissivity factor is included, the dependence of the temperature uncertainty δT on errors in the estimated emissivity is given by

$$\frac{\delta\varepsilon}{\varepsilon} = \rho(x)\frac{\delta T_R}{T}$$

[0096] This shows that the sensitivity to emissivity variations is weaker for blue side measurements (x large). However, moving further into the blue reduces the radiant power and increases the influence of noise. With $\delta T/T$ as a measure of the radiometer sensitivity, and taking the minimum measurable intensity variation $\delta I = H_\nu \Delta\nu$ to be set by the noise level, it can be shown that the maximum sensitivity occurs for $\rho(x) \approx x = 4$, i.e. the centre contour **60** of **Figure 6B**.

Colour pyrometry gives a measure that is relatively insensitive to the radiant efficiency of the material surface, and, though less sensitive to temperature changes than radiometry, is particularly applicable in applications requiring high accuracy. The temperature-dependent shift in the wavelength of the emitted

light may also be sensed by measuring the associated phase shift using dual beam interferometry. The temperature dependence of the interferogram phase for interferometric phase measurements made in a single colour passband are illustrated in **Figures 7A and 7B** respectively showing: the variation of blackbody spectrum as a function of temperature in the range 1500K to 1900K (typical molten iron temperatures); and the variation of the computed interferogram of light passed by the ideal rectangular filter centred on 900nm (at left) as a function of optical delay (MgF2 birefringent plate thickness) and for temperatures in the range 1500K to 1900K. Note the phase change associated with the change in the centre-of-mass of the spectral emission. Although the latter approach has a number of advantages (e.g. high light throughput and compatibility with two dimensional imaging), it has never been applied to the problem of colour pyrometry. It can be shown that the changes in the interferogram phase may be derived from a direct measure of the change in source temperature **[8]**.

[0097] The simplest of the spatial-multiplex coherence-imaging systems uses dual output interferometer ports to sense the change in interferogram phase associated with the shifts in the spectral centre-of-mass of a given scene.

[0098] If the interferogram is being observed at a fringe zero-crossing (this can be arranged by appropriately selecting or tuning the optical path difference), the complementary interferometer outputs will be balanced as shown by curve **80** in **Figure 8**. When the mean colour changes, the interferogram phase correspondingly shifts, thereby giving rise to an imbalance in the detected intensities. To first order, the difference between the images normalized to the mean image intensity gives the interferogram phase shift, and thereby the radiating surface temperature.

[0099] A simple method to generate the complementary images is to use a Wollaston prism to angularly separate the orthogonally polarized outputs of a polarization interferometer as shown in **Figure 9**. The optical components that make up such a system are as follows.

a) The polarization mask consists of a simple polarizer **90** and first image plane iris **91**. These components ensure that only a single image of the scene traverses the interferometer – the orthogonal polarization component is not transmitted.

b) A wideband filter **92** to isolate the spectral region(s) of interest.

c) The radiation traverses a fixed birefringent delay plate **93** having its fast axis at 45° to the plane of polarization of the incoming light **94** from the scene.

d) The Wollaston prism **95** and imaging lens **96** form the final antiphase interferometric images.

e) Detector arrays **97** for detection of the interferometric images.

[00100] An example of the use of this split-image approach is for sensing the change in the spectral centre-of-mass in a single pass-band that attends that change in temperature of a radiating blackbody. The associated changes in the interferogram phase can be shown to be a direct measure of the change in

source temperature. An advantage of this approach over traditional two-colour pyrometer systems is that the images have comparable brightness thereby leading to improved system dynamic range and signal to noise ratio. The use of a single optical passband and polarization interferometer also simplifies optical design. The system phase response needs to be calibrated once against a black or greybody of known temperature. In the former case, it becomes possible to also measure the absolute emissivity.

Image processing algorithm for split image coherence pyrometry

[00101] As already noted, interferometers provide two output ports whose signals are in antiphase – i.e bright and dark interference fringes **80** and **82** respectively of **Figure 8**. The difference in intensity between the two signals (normalized to their average intensity) $q = (S_+ - S_-)/(S_+ + S_-)$ depends on the interferogram phase, and so can be used to estimate temperature changes. For measurements near a fringe zero-crossing **84** (i.e. near where the bright and dark interference fringes intersect for light at centre wavelength λ_0) i.e. the normalized difference between bright and dark fringes near a zero crossing is a close measure of the fringe phase shift. From this measurement, it is straightforward to show that

$$q \approx \zeta \phi \qquad (7)$$

where ζ is the interference fringe amplitude and ϕ is the shift in the interferogram phase produced by the blackbody spectral distribution (the fringe amplitude is weakly temperature dependent). Hereafter, q will be referred to simply as the "coherence".

[00102] It can be shown that the temperature-dependent phase shift is given by **[8]**

$$\phi = -\kappa \beta \Delta\lambda/\lambda_0 \qquad (8)$$

where κ is a constant proportional to the interferometer phase delay offset, $\Delta\lambda$ is the width of the optical passband and λ_0 is the passband centre wavelength.

[00103] For measurements made on the "blue" side of the blackbody peak radiation wavelength, the quantity $\beta = (3 - x)$ is equal to the slope of the blackbody radiation curve and $x = hc/\lambda_0 kT$ is the "blackbody parameter". Thus, it is the sensitivity of the interferogram phase to changes in the spectral slope of the emitted radiation that allows a determination of the source temperature, independent of the source brightness. For small changes in temperature δT about some "target" temperature T_0, a linear relationship is obtained:

$$q = q_0 + \alpha x_0 (\delta T/T_0) \qquad (9)$$

where the proportionality constant, or sensitivity factor α is given by $\alpha = -\zeta \kappa \Delta\lambda/\lambda_0$, $x_0 \equiv (hc/\lambda_0 kT_0)$ is the blackbody parameter at T_0. and q_0 is a calibration constant.

[00104] The sensitivity factor α is most conveniently determined by calibration against a source of known temperature, or through numerical modelling. If the interferometer phase delay offset is chosen for optimum sensitivity to small temperature changes ($\zeta\,\kappa \approx 0.15$) we obtain

$$\alpha \approx -0.15\,\Delta\lambda/\lambda_0 \qquad (10)$$

[00105] Both colour and radiant intensity (brightness) vary with temperature. The theoretical variation of brightness with temperature in a given narrow band is given approximately by

$$\rho \equiv I / I_0 = \varepsilon (T/T_0)^{x_0} \qquad (11)$$

where I_0 is the spectrally-integrated (over passband $\Delta\lambda$) blackbody intensity at T_0 and ε is the surface emissivity. The blackbody intensity is determined by calibration using $I_0=(S_+ + S_-)$ (see Equation (1)).

[0100] The change in brightness $\delta I = I - I_0$ associated with a small temperature change is therefore approximated by

$$\delta I/I_0 = \varepsilon\, x_0\, (\delta T/T_0). \qquad (12)$$

[0101] Comparing Equations (9) and (12), we note that the colour-based temperature estimate is at least a factor $\Delta\lambda/\lambda_0$ less sensitive to temperature changes than the radiometric estimate. The radiometric estimate, however, depends on a knowledge of the surface emissivity.

[0102] Equations (9) and (12) also show that by simultaneously measuring the radiant intensity (brightness) and coherence q, and provided the emissivity is not a function of wavelength, it is possible to estimate both the radiant efficiency of the surface (its emissivity) and the surface temperature. When the emissivity is wavelength dependent, however, one must correct for the emissivity "slope".

[0103] To obtain the coherence offset and sensitivity factors, it is necessary to observe a calibrated blackbody oven. Having correctly registered the left and right split images, for any given region **r** in the calibration image, one can fit a straight line to the measured coherence versus temperature (Equation 2) to obtain the spatially resolved calibration quantities $q_0(\mathbf{r})$ and $\alpha(\mathbf{r})$. Having determined the calibration images, the temperature image is obtained from the shifted and scaled coherence, hereafter called the "normalized coherence":

$$Q \equiv (q - q_0)/\alpha = x_0(\Delta T / T_0)$$

[0104] A sample split-image is shown in **Figure 11** of the molten iron stream at the taphole of Blast Furnace #5 at Bluescope Steel in Port Kembla, Australia. The 50-pixel square box **1100** shows the region over which spatial averages were acquired. **Figure 12** shows the temporal history of the coherence and brightness temperatures in the region **1100** for 200 uncorrelated image frames of the molten iron stream. Note that there is a high degree of correlation between the coherence and brightness estimates (**1200** and **1202** of **Figure 12** respectively). The coherence temperature **70** is generally higher than the brightness temperature **1204** (due to emissivity effects). The good temporal correlation between the independent

brightness and coherence temperature estimates is consistent with the fact that the calculated surface emissivity **1204** varies little over the observation time.

Dual-colour quadrant image coherence pyrometry

[0105] In colour (or coherence) pyrometry it is often be the case that the surface emissivity is also a function of wavelength (emissivity slope) and that this can lead to a false estimate of the colour temperature. In such cases, additional information is required in order to recover the emissivity slope.

[0106] By requiring that the phase shift measurements in adjacent or overlapping spectral bands be consistent – that is, requiring the measurements to yield a consistent temperature – and under the assumption that the emissivity varies linearly with colour across these bands, it is possible in principle to estimate, and so compensate the effects of emissivity slope to obtain a true temperature estimate – at a given temperature, the blackbody spectral tilt in each pass-band is different, while it is assumed that the emissivity slope is the same. The estimate can be improved provided the relative colour-channel sensitivities are known. The optical layout for a quadrant imaging coherence pyrometer suitable for such measurements is shown in **Figures 13A** and **13B** (in elevation and plan view respectively). The optical layout for a quadrant imaging coherence pyrometer **1300** suitable for such measurements is as follows:

a) The polarization mask **1302** consists of a Wollaston (**1304**) / lens (**1306**) / split-field-polarizer (**1308**) combination. Distinct spectral regions of interest are isolated at the two halves of the mask (i.e. beams **1310** and **1312**). Polymer or crystal delay plates can also be introduced at the mask (not shown). The arrangement of the split-field polariser **1308** shown comprises wavelength filters **1314** and **1316** for wavelengths λ_1 and λ_2 respectively, and waveplates **1318** and **1320** with respective delays δ_1 and δ_2.

b) A collimating lens **1322** and bias delay plate (not shown) can be used as required.

c) A final Wollaston prism **1324** (orthogonal to the first prism) forms antiphase coherence images for the two separate passbands, which are imaged onto the image plane **1326** by imaging lens **1328**.

[0107] To prevent the final orthogonally polarized images from overlapping on the detector (not shown) in the image plane, it is possible to limit the lateral extent of the first polarization mask **1102** (in the direction normal to the direction of the image separation). Alternatively, the final images can be isolated using a split-field-polarizer orthogonal to the first (not shown) and then re-imaged onto the detector array.

Image processing algorithm for dual colour coherence pyrometry

[0108] Referring to **Figure 14**, which shows the definition of the various symbols used in the analysis of the pyrometry signal processing algorithm below, when the surface emissivity also varies with wavelength, Equation (8) includes an additional term due to the change in emissivity "colour" $\gamma = (\lambda_0/\varepsilon_0)(\partial\varepsilon/\partial\lambda)|_0 \approx (\Delta\varepsilon/\varepsilon_0)/(\Delta\lambda/\lambda_0)$ where $\Delta\varepsilon$ is the change in emissivity over the passband and ε_0 is the emissivity at λ_0

$$\phi = -\kappa(\beta+\gamma)\,\Delta\lambda/\lambda_0 \qquad (13)$$

[0109] The additional spectral slope factor γ gives rise to an offset in the coherence $q_\varepsilon = -\zeta\kappa\gamma\,\Delta\lambda/\lambda_0$ that mimics a temperature shift. The effect can be estimated by equating q_ε and $\delta q = q - q_0$ (Equation (9)) to obtain

$$(\delta T/T_0)_\varepsilon = \gamma/x_0 \qquad (14)$$

[0110] Taking $x_0 = 10$ (see below), and $\Delta\lambda/\lambda_0 = 0.1$, an emissivity change of 1% across the passband will produce a 1% change in the estimated temperature. This is a problem common to all colour-based pyrometer systems. While two-colour systems are independent of the absolute emissivity ε_0, they are susceptible to slope variations.

[0111] Assuming the e-slope varies in a linear fashion across the passband of interest, it is possible to overcome this problem by making simultaneous split-image measurements in adjacent or nearby bands. This provides essentially four independent equations in three unknowns: the temperature difference δT, mean emissivity, and emissivity slope.

[0112] A simple algorithm to solve for these quantities can be developed as follows. Quantities pertaining to the two passbands are denoted by subscripts 1 or 2. Taking the logarithm of the intensities in the two bands using Equation (11) gives

$$\ln\rho_1 = \ln\varepsilon_1 + x_1\frac{\delta T}{T_0}$$

$$\ln\rho_2 = \ln\varepsilon_2 + x_2\frac{\delta T}{T_0} \qquad (15)$$

[0113] Allowing for the emissivity slope, we obtain the following expressions for the "normalized coherence" in the two bands

$$Q_1 = \gamma_1 + x_1\frac{\delta T}{T_0}$$

$$Q_2 = \gamma_2 + x_2\frac{\delta T}{T_0} \qquad (16)$$

[0114] Where $\gamma_i = \frac{x_i}{\varepsilon_i}\frac{\partial \varepsilon}{\partial x}$ is the logarithmic derivative of the emissivity in each band. Taking the mean and difference of equations (15) and introducing the mean and difference "blackbody parameters" $\bar{x} = (x_2 + x_1)/2$ and $\Delta x = (x_2 - x_1)$ gives

$$\frac{\bar{x}}{\Delta x}(\ln \rho_2 - \ln \rho_1) = \bar{\gamma} + \bar{x}\frac{\delta T}{T_0}$$

$$\frac{1}{\Delta x}(x_2 \ln \rho_1 - x_1 \ln \rho_2) = \ln \bar{\varepsilon} - \frac{\Delta \varepsilon}{\varepsilon} \qquad (17)$$

[0115] Similarly for the normalized coherence, we obtain

$$\frac{1}{2}(Q_2 + Q_1) = \bar{\gamma} + \bar{x}\frac{\delta T}{T_0}$$

$$\frac{\bar{x}}{\Delta x}(Q_2 - Q_1) = \bar{\gamma}(1 - \bar{\gamma}) - \frac{\Delta \varepsilon}{\varepsilon} \qquad (18)$$

where $\bar{\gamma} = \frac{\bar{x}}{\bar{\varepsilon}}\frac{\partial \varepsilon}{\partial x}$.

[0116] Although in the first order approximations applied here, the above equations are approximately linearly dependent, it remains possible to extract information about the e-slope. In practice, the approximation of exactly linear e-slope will be violated, and that noise will compromise the ability to use the additional information provided by adjacent colour bands unless prior information is available. This is a problem common to all colour pyrometer systems. Nevertheless, the ability to simultaneously image the interferometric phase for nearby spectral regions has the potential to yield important additional information in some applications.

Quadrant-image systems - Doppler coherence imaging

[0117] For applications in Doppler spectroscopy, it is possible to estimate species flow and temperature based on the shift and width of an isolated spectral line. In the coherence domain, it is necessary to measure the interferogram phase, contrast and brightness. Previously this information has been obtained using electro-optic modulation of the optical path delay to encode the phase and contrast information in the temporal frequency domain at harmonics of the modulation frequency [6,9].

[0118] For two-dimensional imaging applications, the path delay is electro-optically stepped synchronously with the camera frame rate and the time-multiplexed images unfolded for the unknown quantities [13]. This approach requires that the source properties not change on the time-scale of the camera frame rate (typically 100Hz).

[0119] To acquire the three independent frames of information without the sampling limitations of temporal multiplexing, a quadrant-image approach is required such as that obtained using the optical arrangement of **Figures 13A** and **13B**. In this case, the narrowband spectral filters **1314** and **1316** would be identical while the waveplates **1318** and **1320** would be arranged to have a quarter wave phase difference. Alternatively, waveplate **1318** could be omitted and **1320** would then be a quarter wave plate. A bias delay plate (not shown) would be inserted after the collimating lens **1322**. The image is first split to as to produce vertically separated independent images of the source. These images are then split horizontally by the final Wollaston after passage through the common bias waveplate. **Figure 15** shows such a 4-quadrant image **1500** of a scalpel blade **1502** against the backdrop of interference fringes produced by a 40mm thick lithium niobate waveplate formed under diffuse monochromatic illumination at 488nm. The fine horizontal dividing line **1504** corresponds to the region in the split-field-polarizer where the orthogonally oriented polarizing materials adjoin. The slight horizontal overlap **1506** of the images is a result of the chosen width of the split-field-polarizing plate and the final Wollaston separation angle of approximately 5°. Note the complementarity of the final fringe patterns.

Calibration procedure for quadrature coherence imaging

[0120] To obtain the relative instrument transmission efficiency η_I, fringe visibility (or fringe contrast) ζ_I and phase ϕ_I in each of the 4 quadrants, it is necessary to image a spatially uniform, monochromatic light source that fills the instrument field-of-view. A filtered spectral lamp or laser at wavelength close to that of the emission line of interest coupled to an integrating sphere can be used for this purpose. The interferometer response to a uniform monochromatic light source is then proportional to

$$S_{\pm} = \eta_I[1 \pm \zeta_I \zeta \cos(\phi_I)]$$

[0121] To determine the instrument function the optical phase must be scanned either by slightly tuning the light source wavelength (if this is possible) or by using a fixed wavelength source and scanning the optical path length either thermally or electro-optically. In experiments reported below, we have chosen to step-scan the optical path length through approximately one wave period using a zero-nett-delay electro-optic plate interposed between the birefringent delay plate and final Wollaston. The modulator is constructed of crossed, low-birefringence lithium tantalate (LT) plates each of thickness 10mm. Applying a voltage ramp step-synchronized with the imaging camera frame rate produces a series of images that, in each pixel, captures a sinusoidal intensity pattern that can be numerically fitted to extract the required interferometric parameters. The calibration procedure produces images of transmission efficiency, instrument contrast and phase for each of the four quadrants. For the experiments reported here, typical instrument fringe contrast images for the four quadrants are shown in **Figure 16**. Note the similarity of images within upper and lower pairs. The residual fringe contrast

structure in the top and bottom antiphase pairs is mainly due to incomplete field-widening cancellation of the natural hyperbolic fringe patterns produced by the birefringent plates.

[00106] To verify the calibration, it is necessary to confirm that the instrument transmission and fringe contrast images in each horizontally split pair are closely identical and that their phases differ by π radians. To reduce noise propagation in the demodulation process, the calibration parameter images have been subject to a 5-point median filter and averaged for upper and lower quadrant pairs. The quantities $(\eta_I, \zeta_I, \phi_I)$ for the upper and lower image pairs will be different due to the presence of the quarter wave plate located in one half of the split-field polarizer image mask.

Image processing algorithm for quadrature Doppler coherence imaging

[0122] Before processing the independent images, it is necessary to subtract the background and spatially register each of the four quadrants. In our case, the plasma-illuminated internal toroidal field coils provide a suitable image registration reference.

[0123] After correction for relative transmission efficiency, the signal in corresponding pixels in either of the upper or lower image pairs (for example the upper and lower image pairs of **Figure 19**) is proportional to

$$\begin{aligned} S_{\pm} &= I_0[1 \pm \zeta_I \cos(\phi + \phi_I)] \\ &\equiv I_0[1 \pm \zeta_{Ic}\zeta_c \mp \zeta_{Is}\zeta_s] \\ &\equiv I_0[1 \pm \gamma] \end{aligned}$$

where (I_0, ζ, ϕ) are the emission line brightness, contrast and phase. To simplify notation the instrument complex coherence $[\zeta_{Ic} + i\zeta_{Is} \equiv \zeta_I \exp(i\phi)]$ and plasma complex coherence $[\zeta_c + i\zeta_s \equiv \zeta \exp(i\phi)]$ is introduced and the quantity $\gamma = \zeta_{Ic}\zeta_c \mp \zeta_{Is}\zeta_s$ defined.

[0124] Using superscripts to denote top and bottom images, it is straightforward to extract the complex coherence of the plasma spectral line at the chosen offset delay:

$$\zeta_s = \left(\gamma^{(b)}\zeta_{Ic}{}^{(t)} - \gamma^{(t)}\zeta_{Ic}{}^{(b)}\right)/\Delta$$

$$\zeta_c = \left(\gamma^{(b)}\zeta_{Is}{}^{(t)} - \gamma^{(t)}\zeta_{Is}{}^{(b)}\right)/\Delta$$

[0125] The quantity Δ is related to the degree of orthogonality between the upper and lower image pairs and is given by:

$$\Delta = \left(\zeta_{Is}{}^{(t)}\zeta_{Ic}{}^{(b)} - \zeta_{Is}{}^{(b)}\zeta_{Ic}{}^{(t)}\right) = \zeta_I{}^{(t)}\zeta_I{}^{(b)}\cos\left(\phi_I{}^{(t)} - \phi_I{}^{(b)}\right)$$

Figure 17 shows an image of the quantity $\sin\left(\phi_I{}^{(t)} - \phi_I{}^{(b)}\right)$ that indicates a high degree of quadrature between the top and bottom image sets.

Example results for quadrature Doppler coherence imaging system

[0126] To confirm the performance of the static system, measurements were undertaken on low field (0.1T) rf-heated (70MHz, 80kW) argon discharges in the H-1 heliac at the Australian National University. H-1 is a moderate-scale (1m major radius, 25cm minor radius) toroidal magnetic plasma confinement device. The discharge conditions are similar to those for Doppler imaging results reported using the electro-optically modulated camera [6,9]. A direct view along the major axis of the plasma was available for this work. A schematic of the optical layout, together with an AUTOCAD model of the camera view of the plasma region looking through the vacuum tank port, is shown in **Figures 18A** and **18B** respectively. The vertical structures **1810** of **Figure 18B** are the inside surfaces of the toroidal field coils (TFCs). The curved structure **1820** is the helical field coil (HFC) which sits atop the central poloidal field coil **1830**. The plasma sits above the HFC **1820** and is contained with the TFCs **1810**.

[0127] Figure **19** shows a typical camera snapshot of the plasma with an exposure time of 50 ms. In each quadrant, illuminated by the plasma ion light at 488nm, are two of the 36 internal toroidal field coils (TFCs) and their clamps. At the top of each image is the outline of the helical conductor. Each of the images is inverted so that the plasma actually resides above this conductor and is enclosed by the TFCs. Notice the presence of strong specular reflections from the leftmost of the TFCs in the image.

[0128] The extracted brightness, temperature and flow speed images for an argon discharge at 0.12T in standard magnetic configuration and for a 30mm lithium niobate delay plate (chosen for sensitivity to ion temperatures near 20 electron volts) are shown in **Figure 20**. A 5-pixel median filter has been applied to the temperature and flow images. The static system reproduces all of the features obtained in earlier measurements using the electro-optic camera: the ion temperature profile is substantially hollow while the flow approximates rigid rotation. It can clearly be seen hat the brightness, temperature and flow images show little evidence of cross-coupling.

It will be appreciated that the methods and apparatus described/illustrated above at least substantially provide a multi-coherence imaging system.

[0129] The multi-coherence imaging systems and methods described herein, and/or shown in the drawings, are presented by way of example only and are not limiting as to the scope of the invention. Unless otherwise specifically stated, individual aspects and components of the multi-coherence imaging systems and methods may be modified, or may have been substituted therefore known equivalents, or as yet unknown substitutes such as may be developed in the future or such as may be found to be acceptable substitutes in the future. The multi-coherence imaging systems and methods may also be modified for a variety of applications while remaining within the scope and spirit of the claimed invention, since the range of potential applications is great, and since it is intended that the present multi-coherence imaging systems and methods be adaptable to many such variations.

REFERENCES

[1] T. Vo-Dinh, V. Cullum, and P. Kasili, J. Phys. D: Appl. Phys. **36**,1663 (2003).

[2] The "Mechelle" spectrograph by Andor Technolgy http://www.andor.com/products/spectrographs/?product=ME5000

[3] J.H. Mooney, V.E. Vickers, M. An, and A. Brodzik, J. Opt. Soc. Am. A **14**, 2951 (1997).

[4] P. Jacquinot, J. Opt. Soc. Am. **44**, 761 (1954).

[5] B.A. Patterson *et al.*, Opics Communications **130**, 1 (1996).

[6] J. Howard, C. Michael, F. Glass, and A. Danielsson, Plasma Phys. Control Fusion **45**, 1143 (2003).

[7] J. Howard, Plasma Phys. Control. Fusion, **41** 271 (1999)

[8] J Howard, US patent #7001068, "Method and apparatus for the estimation of the temperature of a blackbody radiator"

[9] J. Howard, C. Michael, F. Glass, and A. Cheetham, Rev. Sci. Instrum. **72**,888 (2001).

[10] W. Steel, *Interferometry* (Cambridge University Press, Cambridge, 1967).

[11] I Solc, J. Opt. Soc. Am. **55**, 621 (1965)

[12] G. Shabtay *et al.*, Optics Express **10**, 1534 (2002)

[13] Chung, J. and Konig, R. and Klinger, T. and Howard, Plasma Phys. Control. Fusion, 47, 919 (2005)

THE CLAIMS DEFINING THE INVENTION ARE AS FOLLOWS:

1. A polarizing image mask for providing angularly multiplexed, dual orthogonal polarized beams, each beam being a replica of an incoming radiation beam from a source, the polarising image mask comprising:

a first Wollaston prism as a first polarizing component for providing angularly multiplexed radiation beams from the incoming radiation beam, the beams being multiplexed in a first direction; and

a split field polarizer comprising adjoining, orthogonally oriented polarizing materials for providing angularly multiplexed, dual orthogonal polarized radiation beams.

2. A polarizing image mask as claimed in claim 1 further comprising an optical power element thereby to produce dual, orthogonally polarized images in the image plane of the optical power element.

3. A polarizing image mask as claimed in claim 2 wherein the split-field-polarizer is located in the image plane of the optical power element thereby to isolate the orthogonally polarized images.

4. A polarizing image mask as claimed in any one of claims 1 to 3 wherein the angularly multiplexed orthogonally polarized radiation beams are passed through respective polarization interferometer optics.

5. A polarizing image mask as claimed in any one of claims 1 to 4 wherein the angularly multiplexed orthogonal polarization images are independently manipulated at the polarized image mask in accordance with requirements.

6. A polarizing image mask as claimed in any one of claims 1 to 5 further comprising at least one colour filter to isolate a spectral region of interest.

7. A polarizing image mask as claimed in claim 1 wherein the split-field-polarizer is fabricated using standard deposition techniques and custom manufactured in accordance with requirements.

8. A polarizing image mask as claimed in any one of claims 1 to 6 further comprising a quarter wave plate inserted in one of the orthogonally polarized images at the polarization mask thereby to introduce a 90 degree relative phase shift between the orthogonally polarized images.

9. A polarizing image mask as claimed in any one of claims 1 to 8 further comprising a second Wollaston prism aligned substantially orthogonal to the first Wollaston prism for further angularly multiplexing the angularly multiplexed orthogonal polarization radiation beams in a second direction.

10. A polarizing image mask as claimed in claim 9 wherein the second direction is substantially orthogonal to the first direction.

11. A method for providing angularly multiplexed, dual orthogonal polarized beams, each beam being a replica of an incoming radiation beam from a source, the method comprising:

providing angularly multiplexed radiation beams from the incoming radiation beam, with a first polarizing component, the beams being multiplexed in a first direction; and

providing angularly multiplexed, dual orthogonal polarized radiation beams with a split field polarizer comprising adjoining, orthogonally oriented polarizing materials.

12. A method as claimed in claim 11 wherein the fist polarizing component is a Wollaston prism.

13. A method as claimed in claim 11 further comprising the step of introducing a 90 degree relative phase shift between the orthogonally polarized images.

14. A method as claimed in claim 11 further comprising the step of angularly multiplexing the orthogonal polarization radiation beams in a second direction.

15. An image forming system capable of acting upon an incoming radiation beam from a source, the system comprising:

a polarization mask comprising a first Wollaston prism as a first polarizing component and a split field polarizer comprising adjoining, orthogonally oriented polarizing materials, the polarisation mask producing dual orthogonal polarized beams which are angularly multiplexed in a first direction;

a polarization element for providing images of each of the dual angularly multiplexed orthogonal polarized on an imaging detector array.

16. An image forming system as claimed in claim 15 further comprising an electro-optical delay switch for switching the optical path delay in accordance with requirements.

17. An image forming system as claimed in claim 16 further comprising a collimating optical power element for collimating the angularly multiplexed dual orthogonal polarized beams

18. An image forming system as claimed in claim 16 wherein the delay switch is formed from a ferroelectric liquid crystal compound.

19. An image forming system as claimed in claim 16 wherein the imaging detector array has an image frame rate, and wherein the delay switch is synchronised with the frame rate of the detector array.

20. An image forming system as claimed in either claim 15 or 19 wherein the imaging detector array is selected from a charge coupled device camera or a framing streak camera or other multi-element detection device.

21. An image forming system as claimed in claim 15 wherein the polarization element comprises a second Wollaston prism aligned substantially orthogonal to the first Wollaston prism for further angularly multiplexing the angularly multiplexed orthogonal polarization radiation beams in a second direction.

22. An image forming system as claimed in any one of claims 15 to 21 further comprising at least one filter for providing a coherence image of desired spectral content to be imaged on the detector array.

23. An image forming system as claimed in any one of claims 15 to 21 further comprising a plurality of filters, each filter transmitting an independent spectral pass bands for providing coherence images of distinct spectral content to be imaged on the detector array.

24. An image forming system as claimed in claim 22 or 23 wherein the filter is selected from dichroic or interference filters.

25. An image forming system as claimed in claim 22 or 23 wherein the filter is incorporated into the polarization mask.

26. An image forming system as claimed in any one of claims 15 to 25 further comprising a polarization stage and imaging optical power element to image each of the angularly multiplexed information into spatial distinct images on the detector array.

27. An image forming system as claimed in claim 26 wherein the polarization stage is selected from a simple polarizer, a Wollaston prism, or a further polarization mask.

28. A spatio-temporal multiplex optical system comprising:

a polarizing image mask comprising:

a first Wollaston prism for providing angularly multiplexed radiation beams from the incoming radiation beam, the beams being multiplexed in a first direction; and

a split field polarizer comprising adjoining, orthogonally oriented polarizing elements for providing angularly multiplexed, dual orthogonal polarized radiation beams;

a collimating optical power element;

an optical delay switch for modifying the polarization of the angularly multiplexed, dual orthogonal polarized radiation beams;

a second Wollaston prism for providing further angularly multiplexed radiation beams from the angularly multiplexed, dual orthogonal polarized radiation beams, the beams being further angularly multiplexed in a second direction;

a detector array for receiving each of the four angularly multiplexed radiation beams; and

an imaging optical power element for focusing the four angularly multiplexed radiation beams to respective substantially spatially distinct region of the detector array.

29. A polarizing image mask substantially as herein described with reference to any one of the embodiments of the invention illustrated in the accompanying drawings.

30. An image forming system substantially as herein described with reference to any one of the embodiments of the invention illustrated in the accompanying drawings.

31. A spatio-temporal multiplex optical system substantially as herein described with reference to any one of the embodiments of the invention illustrated in the accompanying drawings.

PRIOR ART

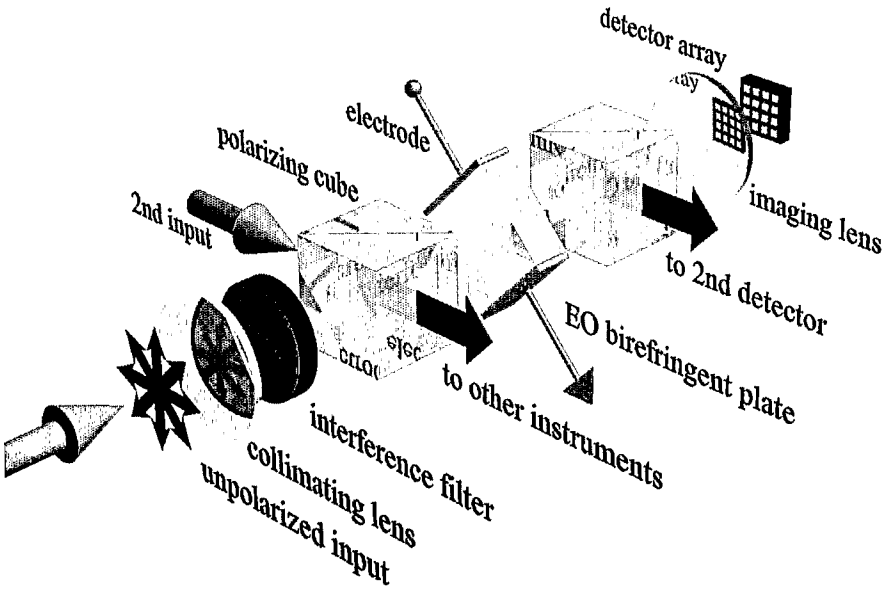

FIGURE 1

PRIOR ART

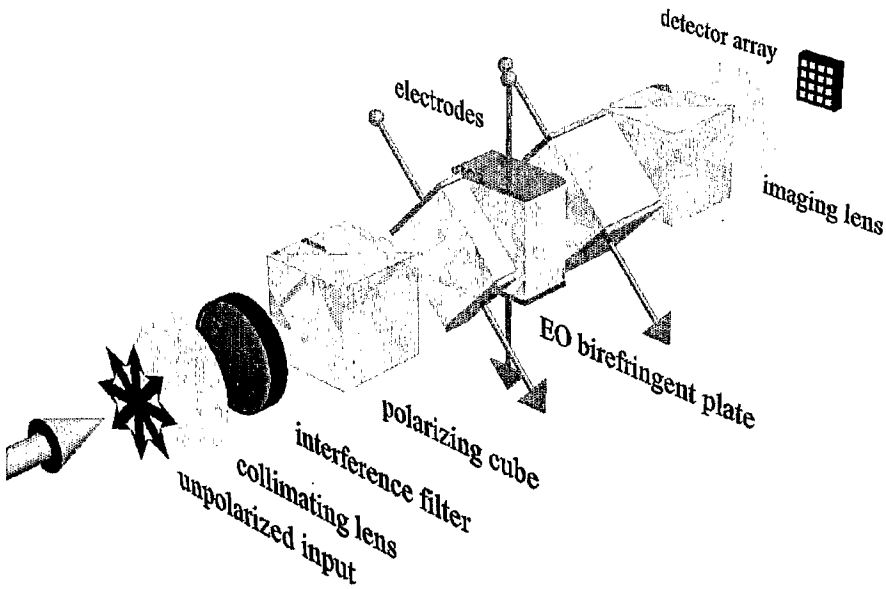

FIGURE 2

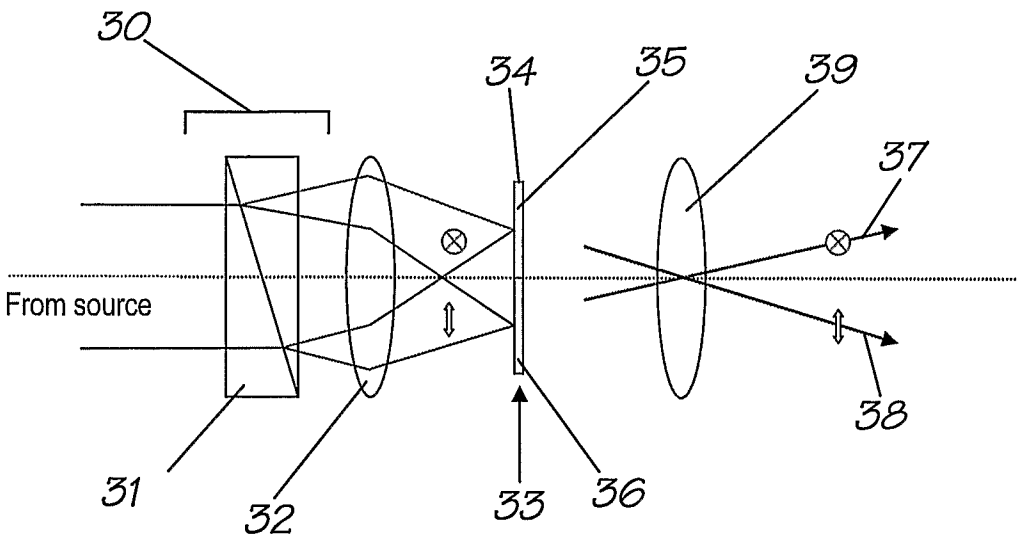

FIGURE 3

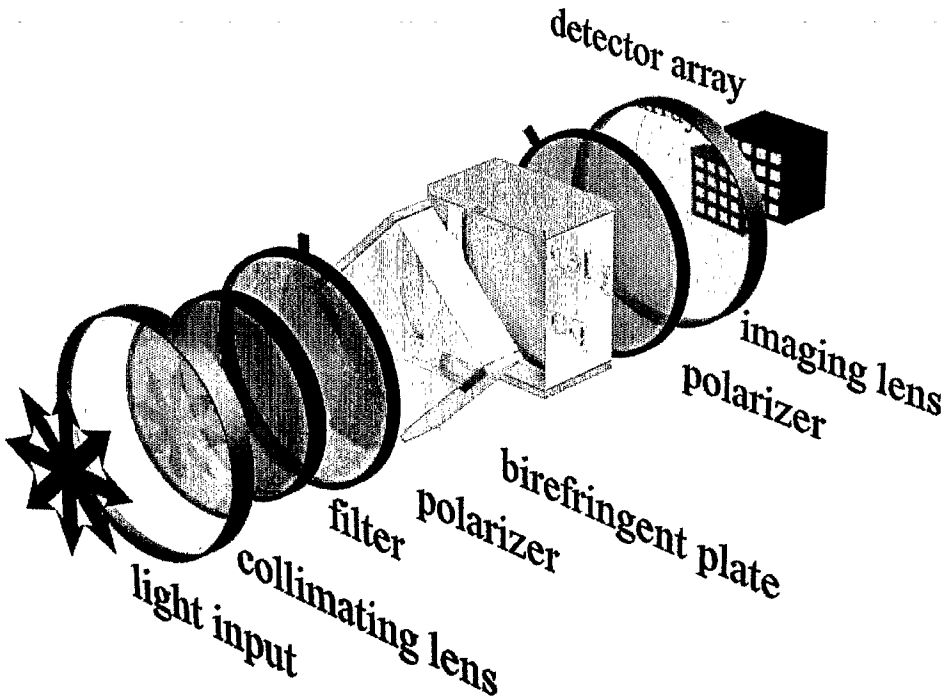

FIGURE 4

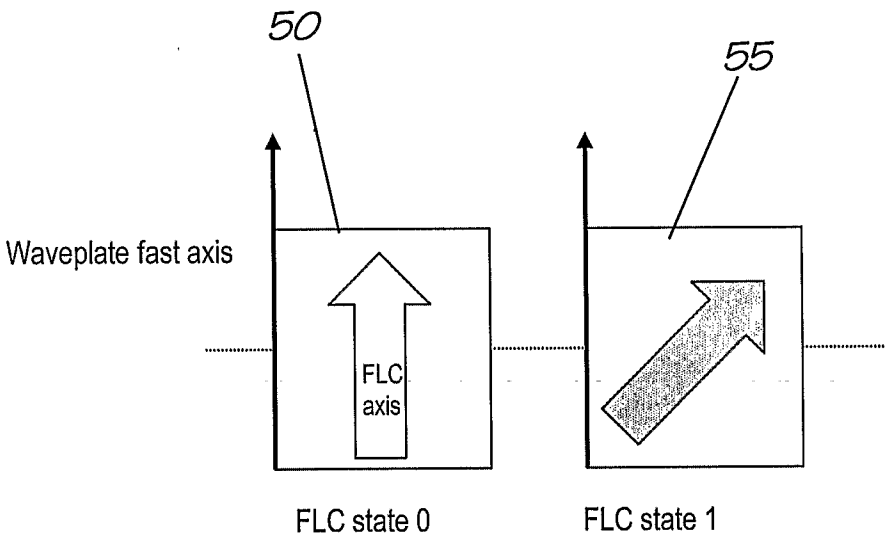

FIGURE 5

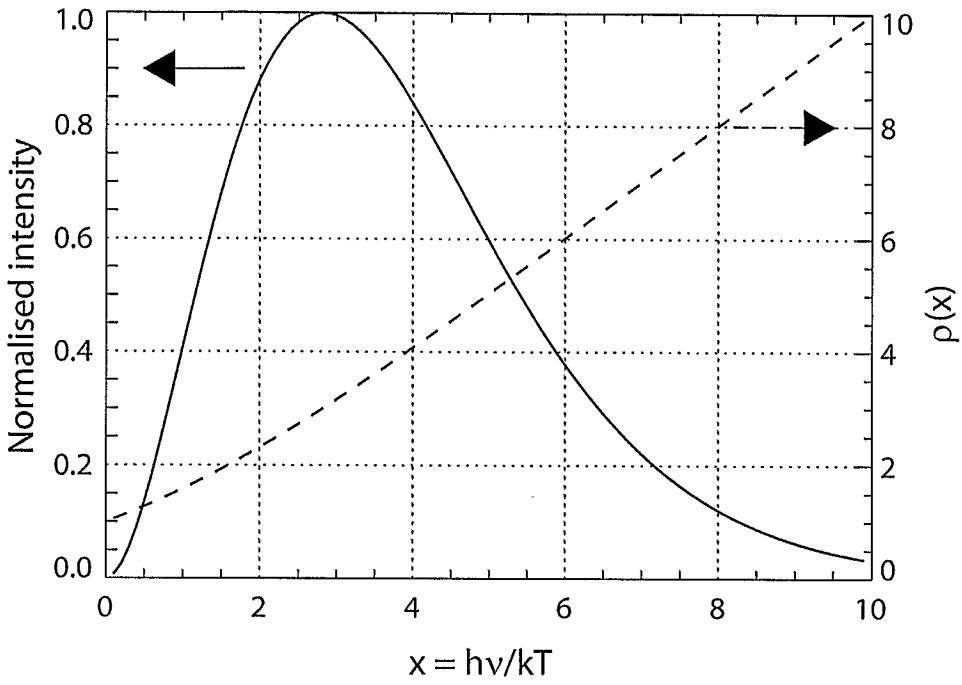

FIGURE 6A

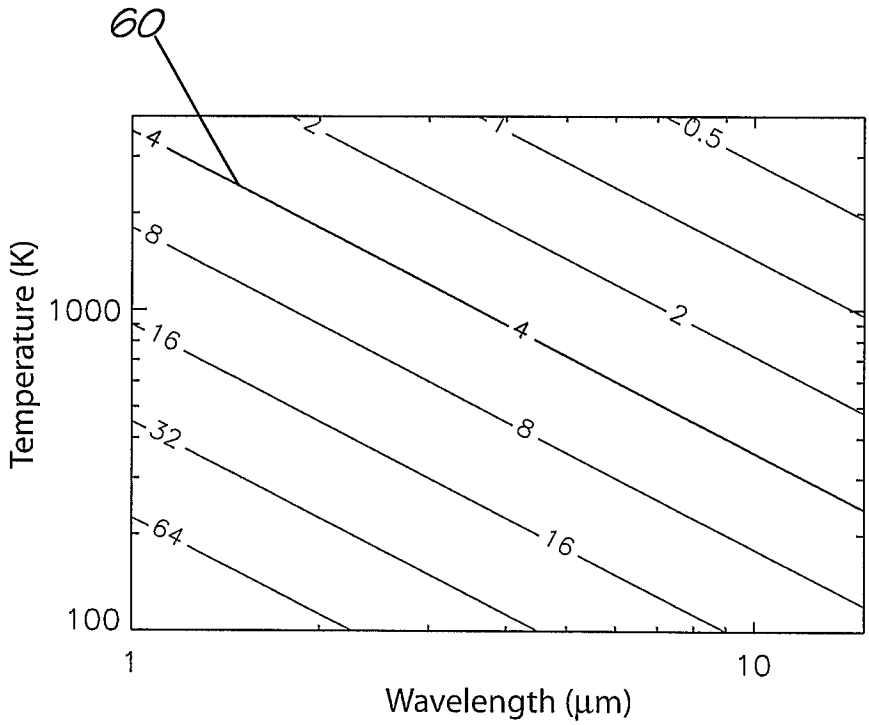

FIGURE 6B

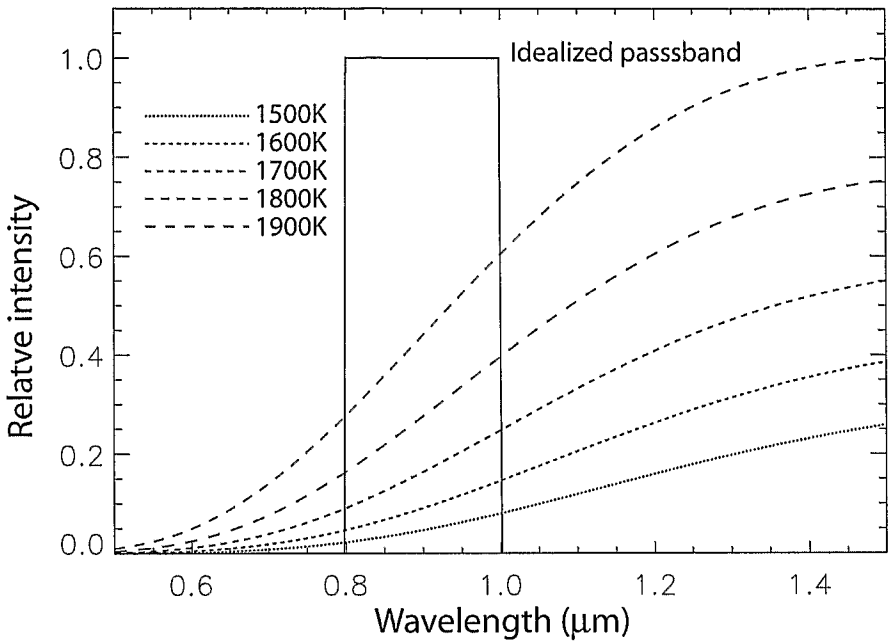

FIGURE 7A

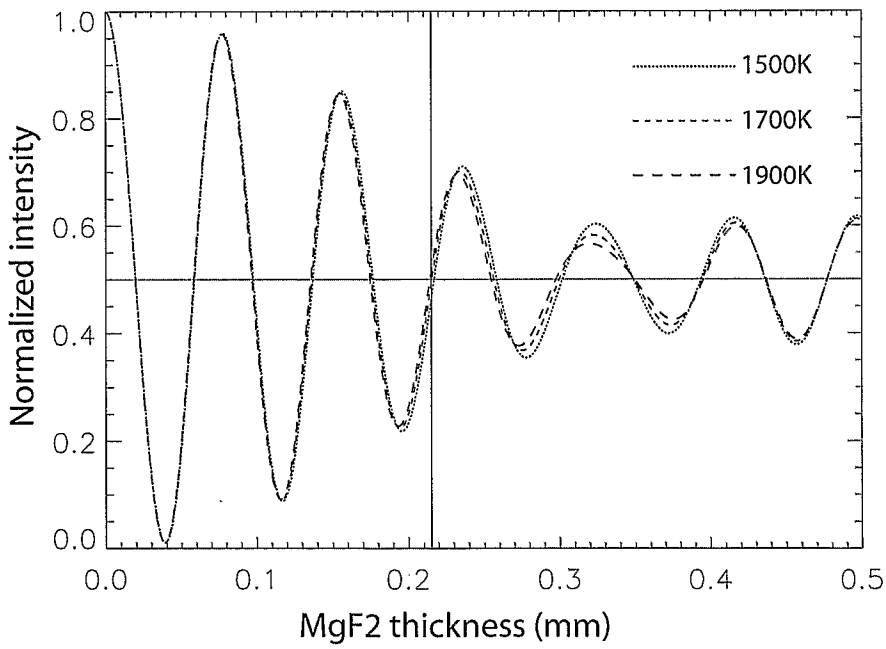

FIGURE 7B

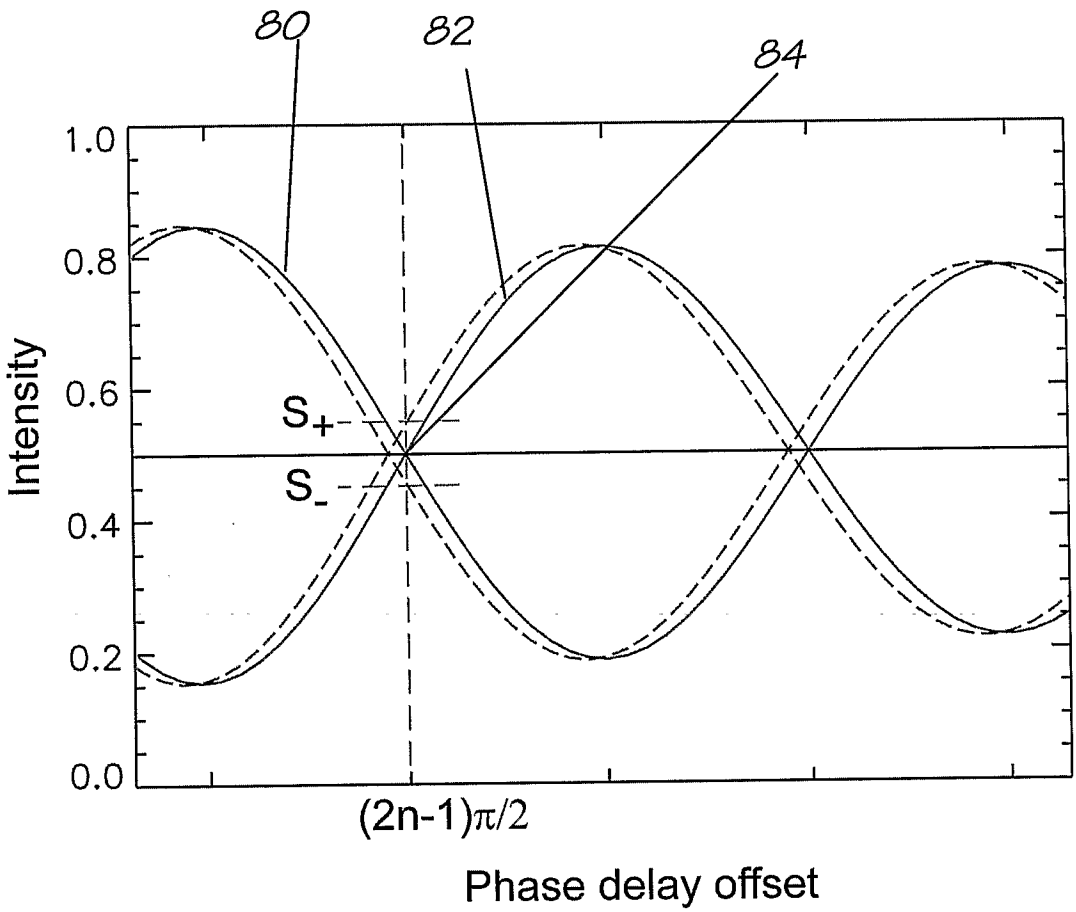
80
82
84
1.0
0.8
0.6
0.4
0.2
0.0
Intensity
S+
S-
(2n-1)π/2
Phase delay offset

FIGURE 8

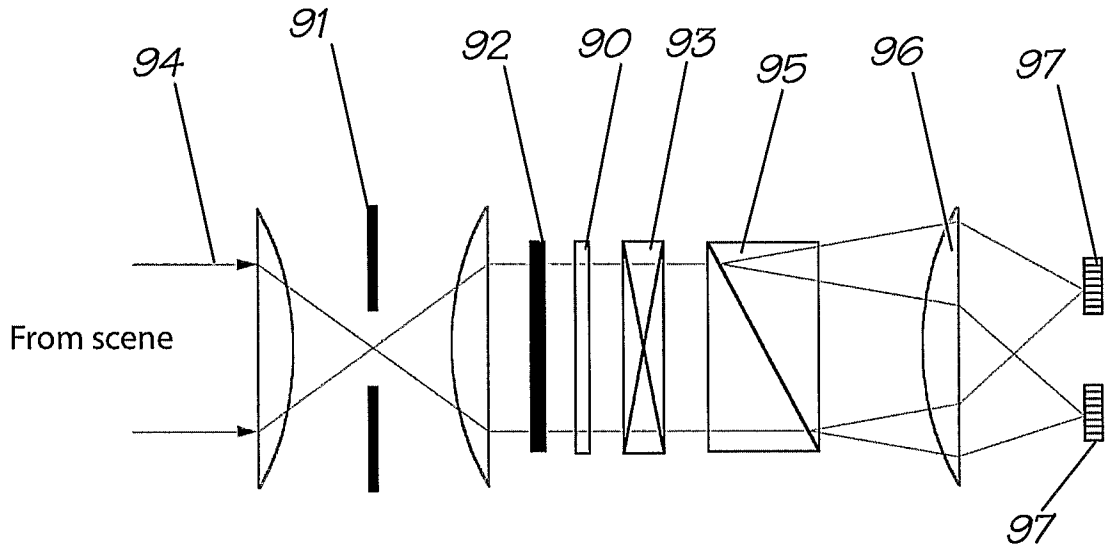

FIGURE 9

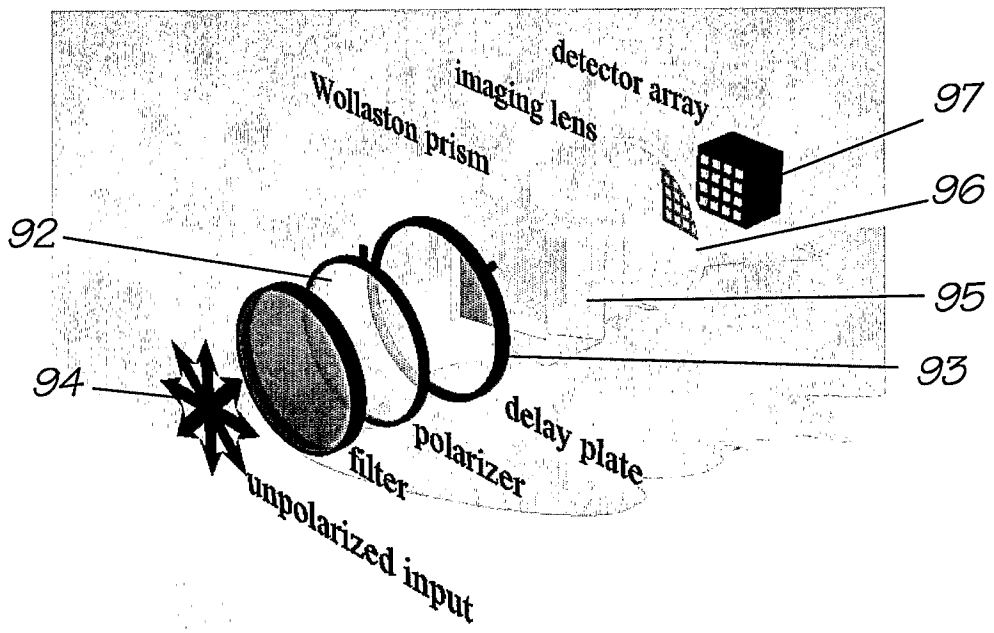

FIGURE 10

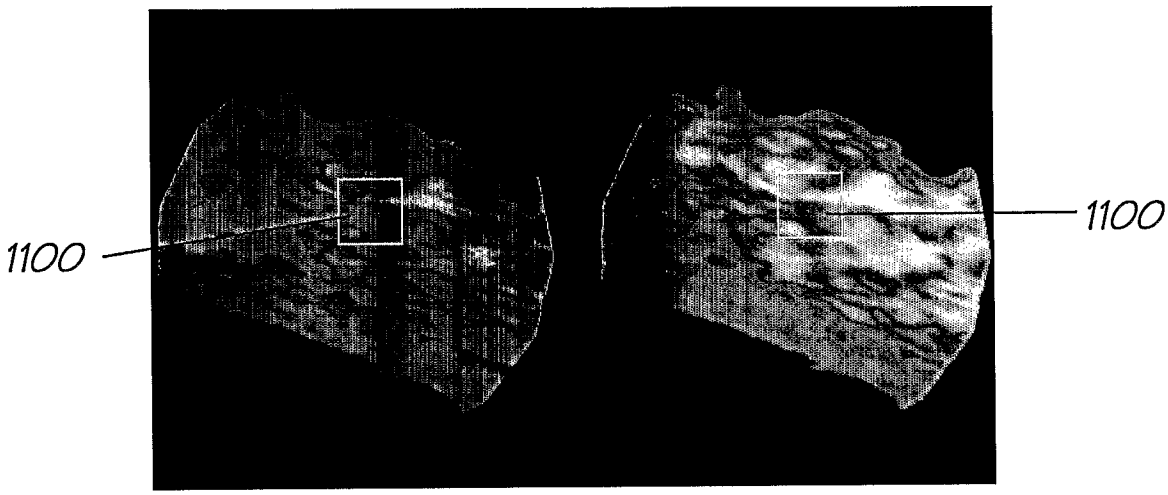

FIGURE 11

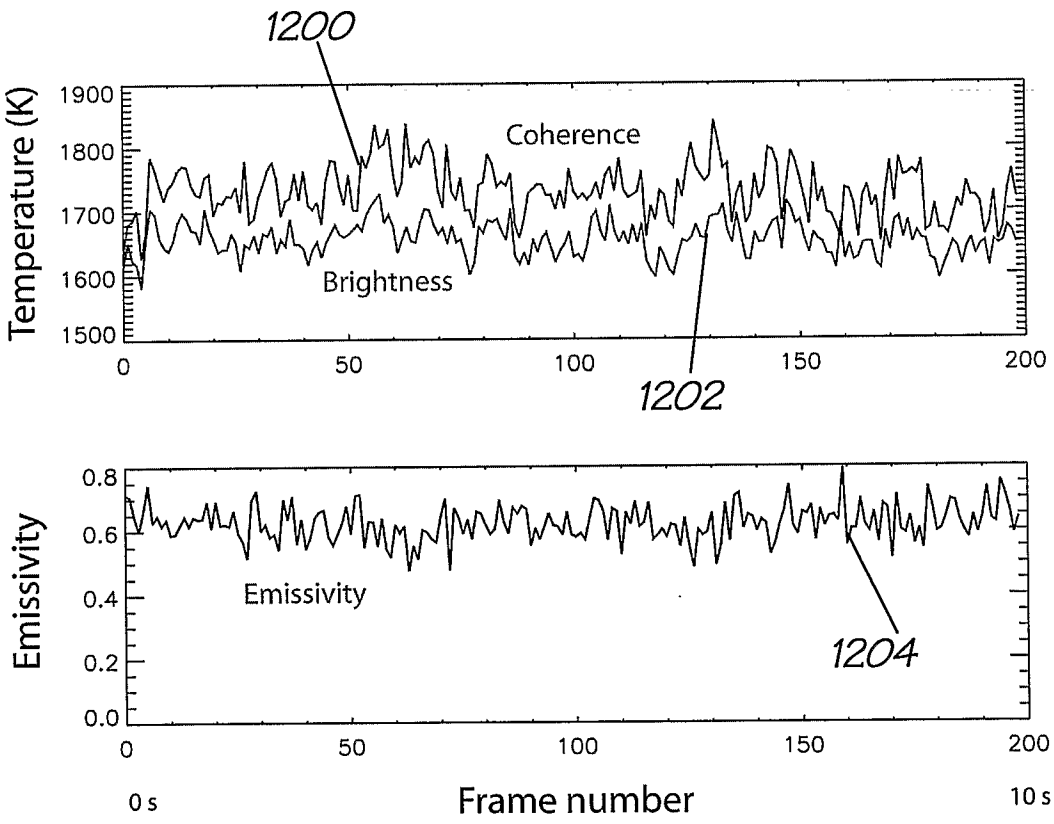

FIGURE 12

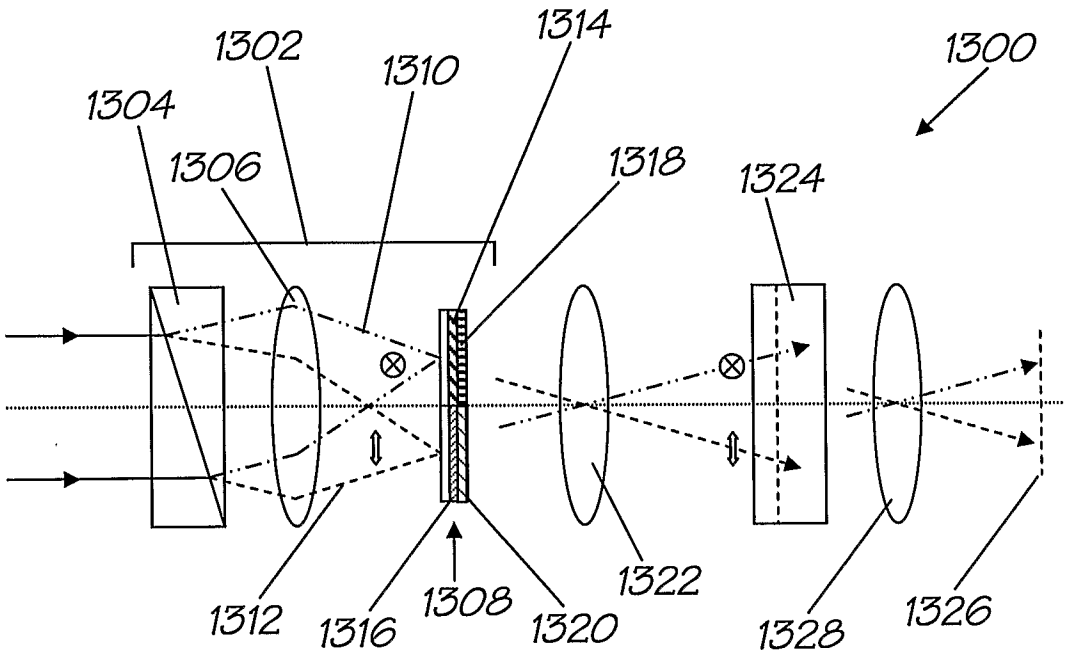

FIGURE 13A

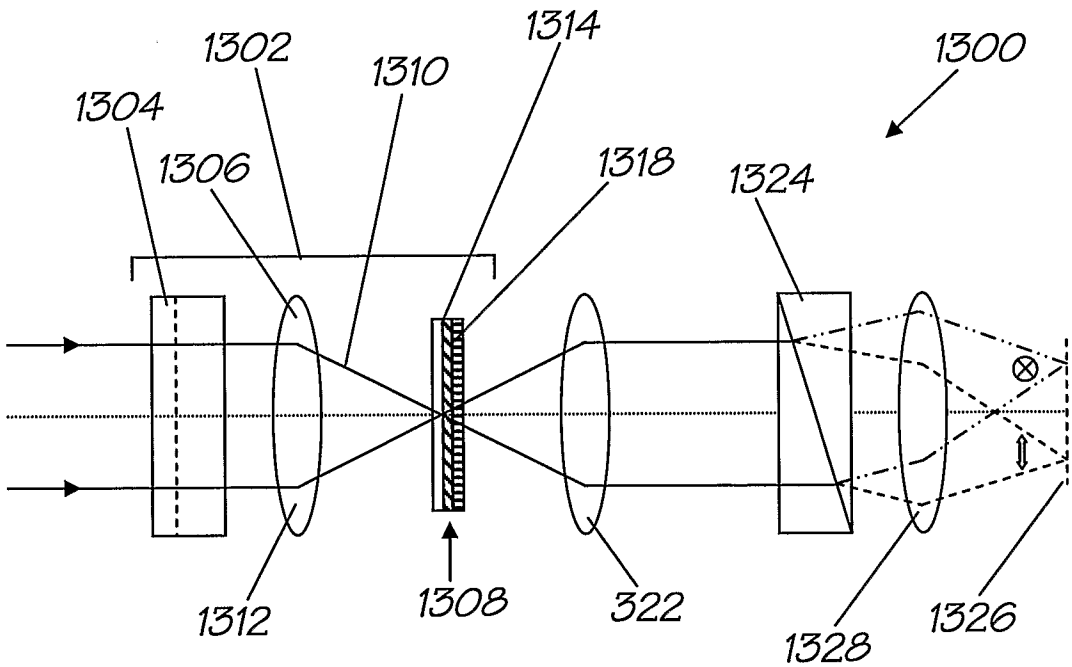

FIGURE 13B

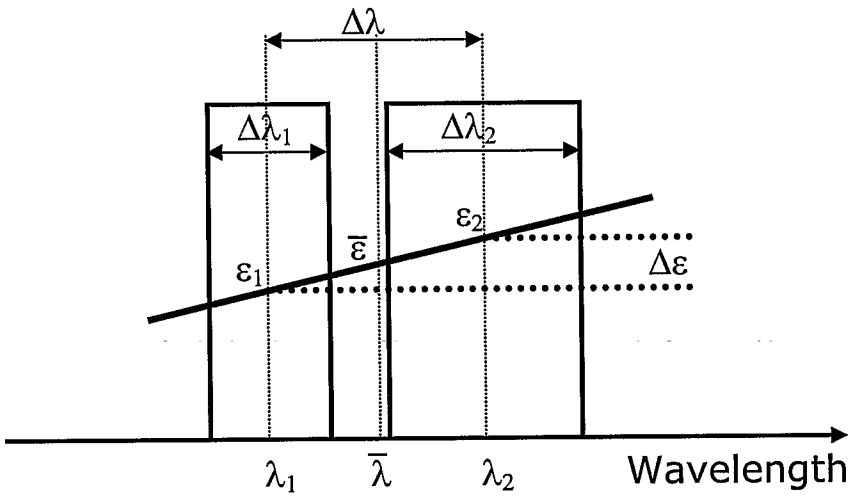

FIGURE 14

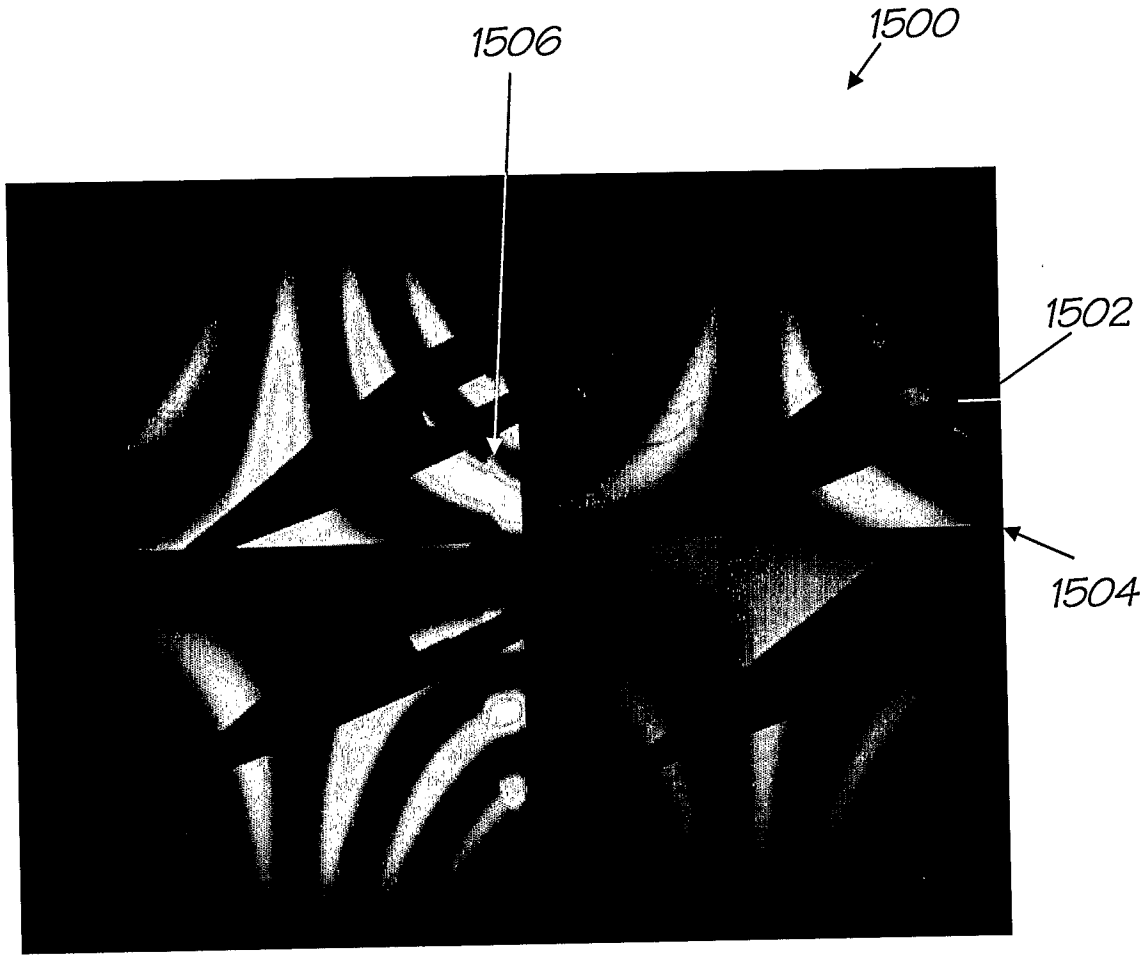

FIGURE 15

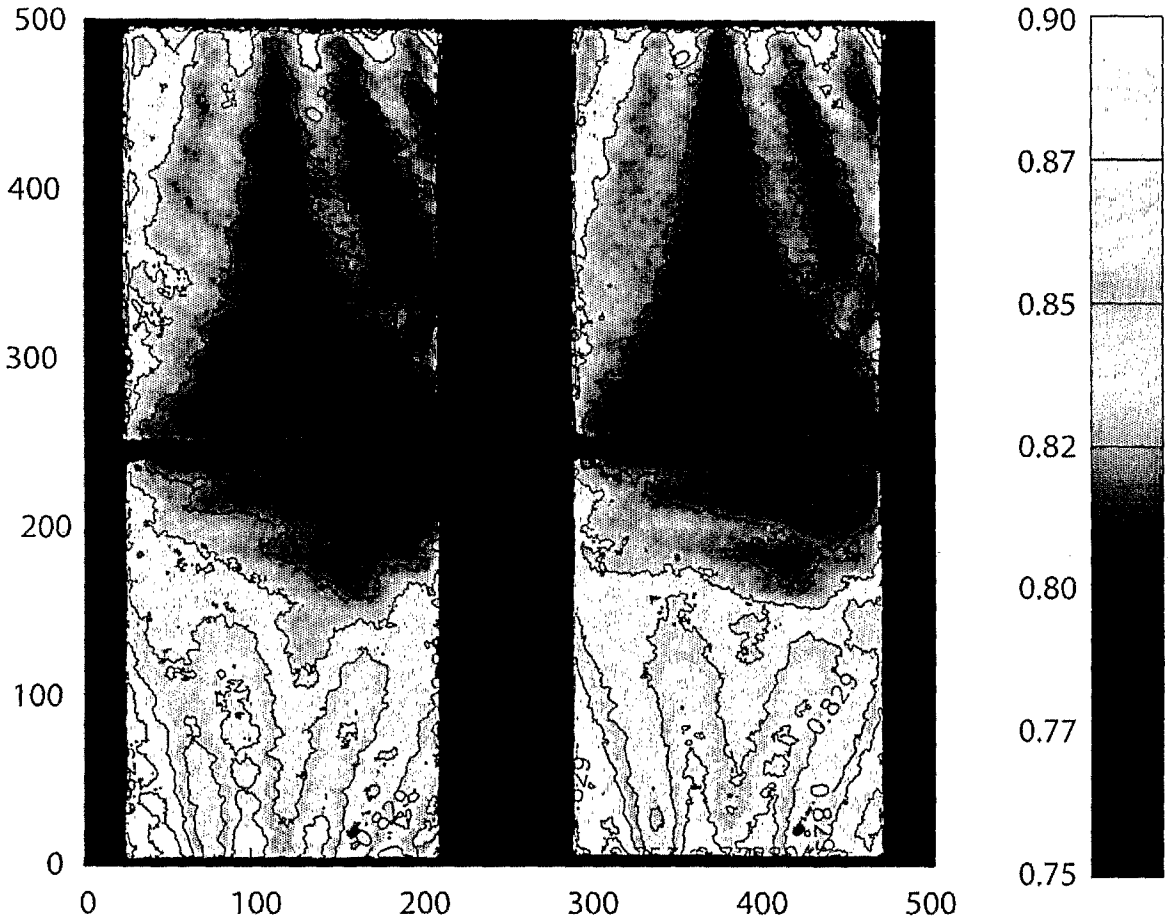
500
400
300
200
100
0
0
100
200
300
400
500
0.90
0.87
0.85
0.82
0.80
0.77
0.75

FIGURE 16

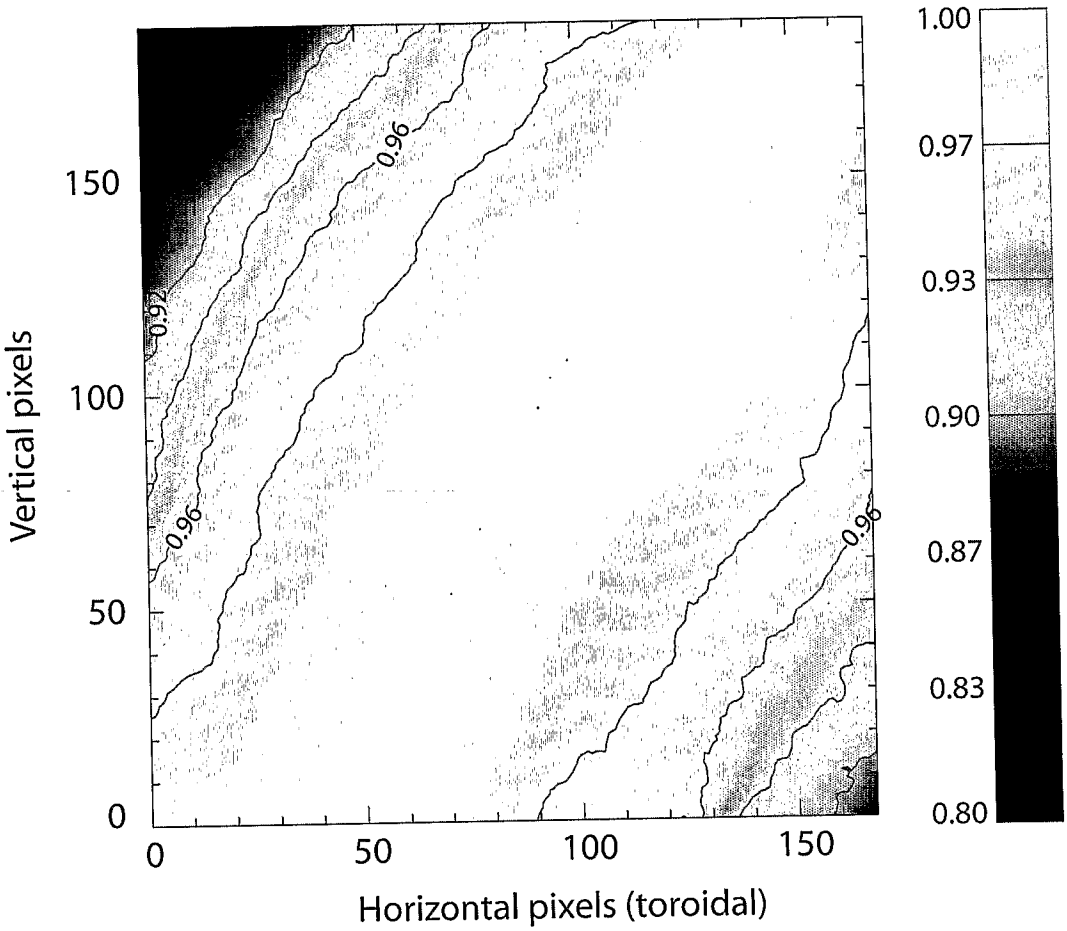
Vertical pixels
Horizontal pixels (toroidal)
0
50
100
150
0.92
0.96
0.96
0.96
1.00
0.97
0.93
0.90
0.87
0.83
0.80

FIGURE 17

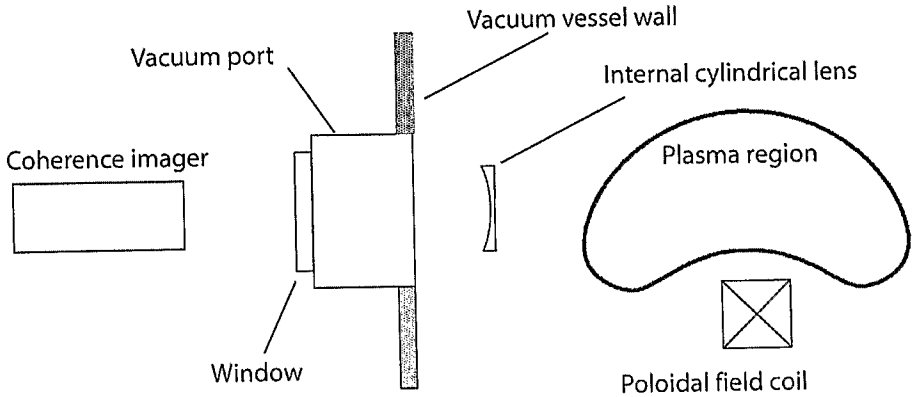

FIGURE 18A

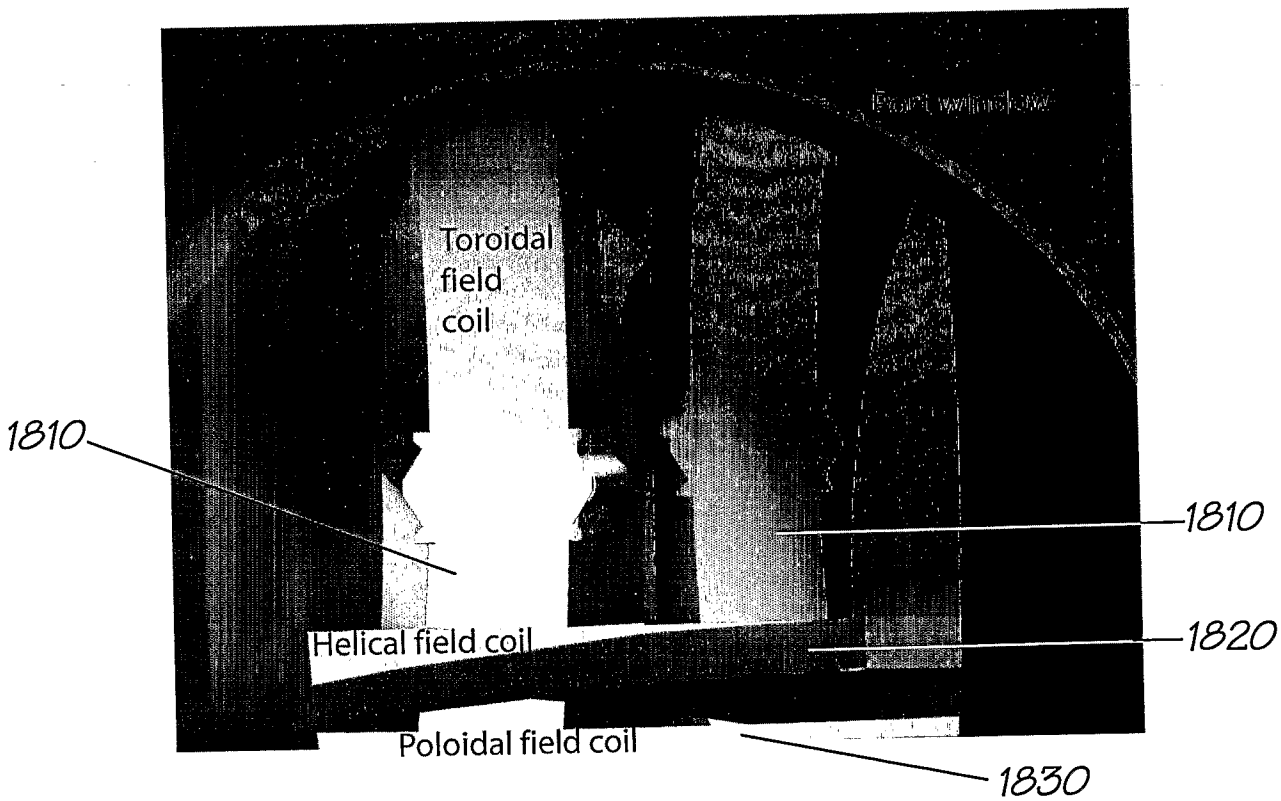

FIGURE 18B

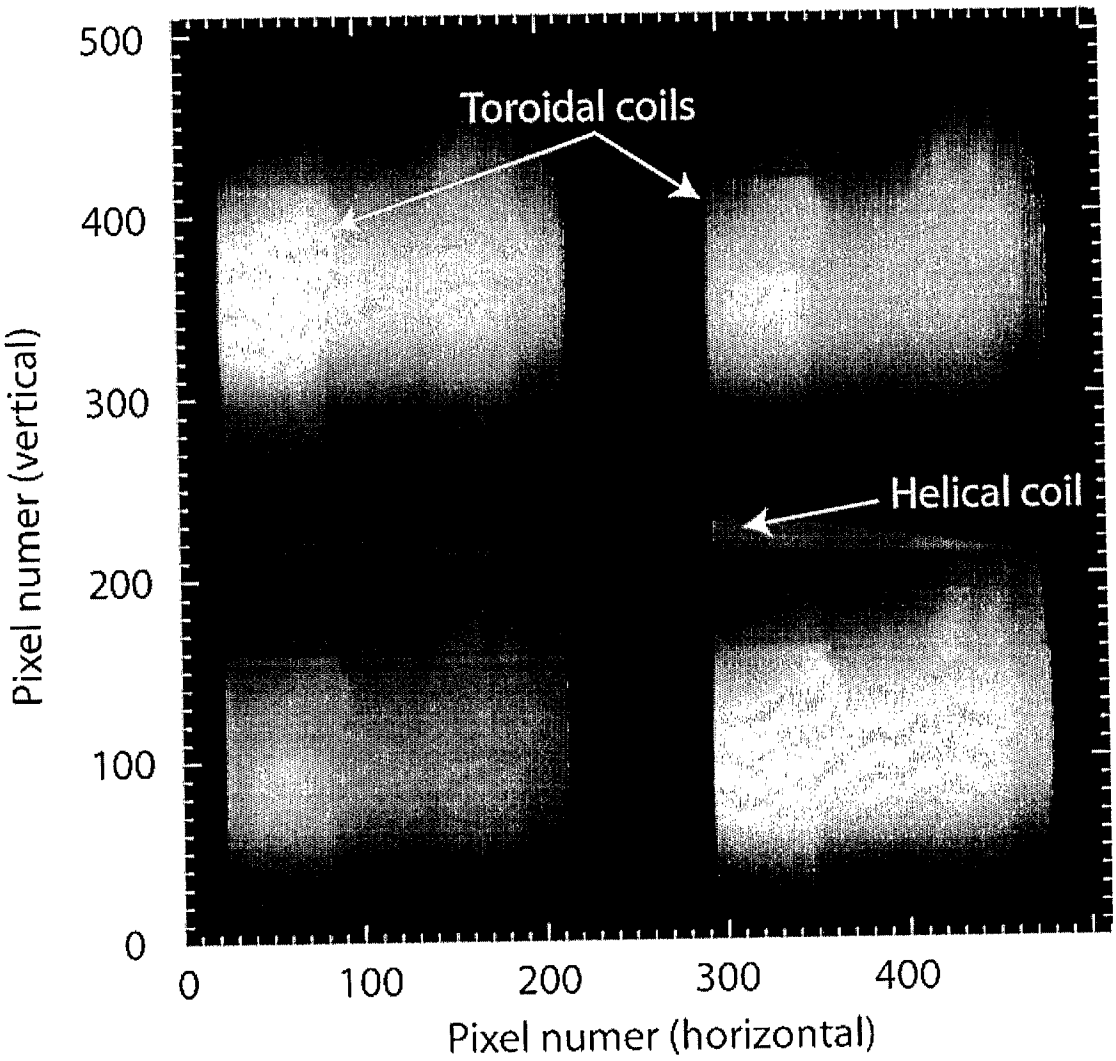
Toroidal coils
Helical coil
Pixel numer (vertical)
Pixel numer (horizontal)
500
400
300
200
100
0
0
100
200
300
400

FIGURE 19

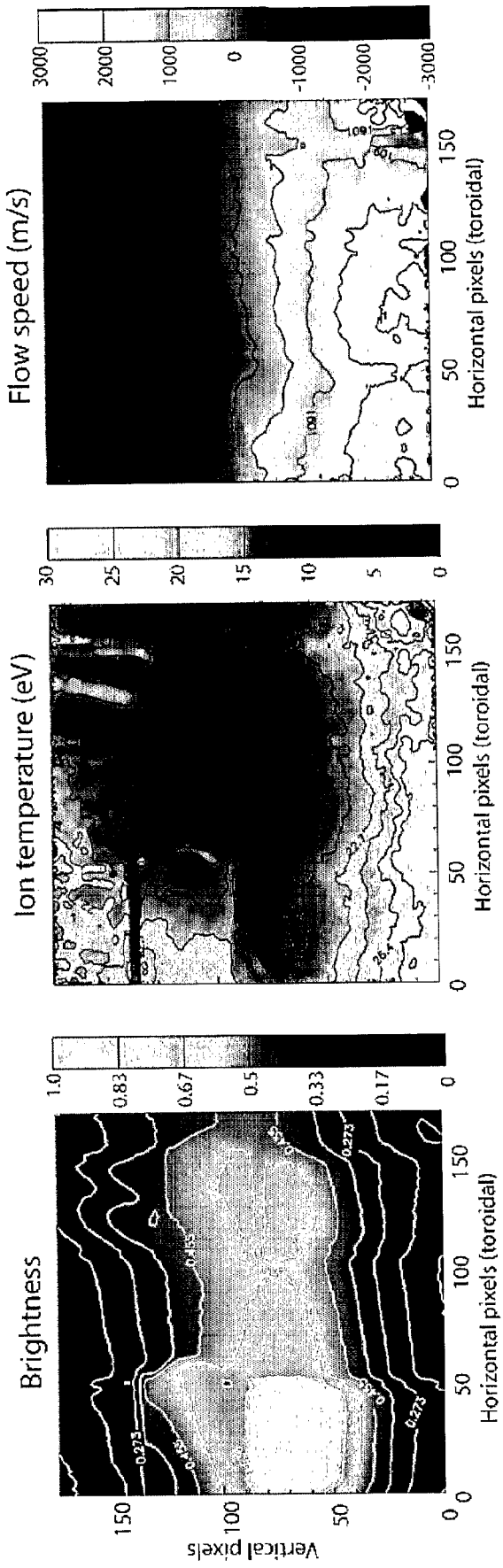
Brightness
Vertical pixels
Horizontal pixels (toroidal)
1.0
0.83
0.67
0.5
0.33
0.17
0
Ion temperature (eV)
Horizontal pixels (toroidal)
30
25
20
15
10
5
0
Flow speed (m/s)
Horizontal pixels (toroidal)
3000
2000
1000
0
-1000
-2000
-3000

FIGURE 20

INTERNATIONAL SEARCH REPORT

International application No.
PCT/AU2006/001397

A. CLASSIFICATION OF SUBJECT MATTER

Int. Cl.

G02B 5/30 (2006.01) *G01J 5/58* (2006.01) *H04J 14/06* (2006.01)

According to International Patent Classification (IPC) or to both national classification and IPC

B. FIELDS SEARCHED

Minimum documentation searched (classification system followed by classification symbols)

Documentation searched other than minimum documentation to the extent that such documents are included in the fields searched

Electronic data base consulted during the international search (name of data base and, where practicable, search terms used)
DWPI and keywords: polarised; wollaston, nicol, prism, birefringent, calcite; split field; angle; multi, separation; multiplex, composite, multispectral, coherence; temporal, time, delay; and other similar terms

C. DOCUMENTS CONSIDERED TO BE RELEVANT

Category*	Citation of document, with indication, where appropriate, of the relevant passages	Relevant to claim No.
X	EP 1519170 A1 (RAYTHEON COMPANY) 30 March 2005 See paragraphs [0020] – [0031], figure 2 and figure 5	1-15,20-27,29,30
X	US 6212313 B1 (LI) 3 April 2001 See abstract and column 3 line 60 – column 5 line 45	1, 5-14
X	US 5135183 A (WHITNEY) 4 August 1992 See column 3 line 47 – column 4 line 55	1-3,6,7,11,12,15, 20,22,23,26,29,30

[X] Further documents are listed in the continuation of Box C [X] See patent family annex

* Special categories of cited documents:

"A" document defining the general state of the art which is not considered to be of particular relevance

"E" earlier application or patent but published on or after the international filing date

"L" document which may throw doubts on priority claim(s) or which is cited to establish the publication date of another citation or other special reason (as specified)

"O" document referring to an oral disclosure, use, exhibition or other means

"P" document published prior to the international filing date but later than the priority date claimed

"T" later document published after the international filing date or priority date and not in conflict with the application but cited to understand the principle or theory underlying the invention

"X" document of particular relevance; the claimed invention cannot be considered novel or cannot be considered to involve an inventive step when the document is taken alone

"Y" document of particular relevance; the claimed invention cannot be considered to involve an inventive step when the document is combined with one or more other such documents, such combination being obvious to a person skilled in the art

"&" document member of the same patent family

Date of the actual completion of the international search	Date of mailing of the international search report
15 November 2006	23 NOV 2006
Name and mailing address of the ISA/AU AUSTRALIAN PATENT OFFICE PO BOX 200, WODEN ACT 2606, AUSTRALIA E-mail address: pct@ipaustralia.gov.au Facsimile No. (02) 6285 3929	Authorized officer **LYNN BLOOMFIELD** Telephone No : (02) 6283 2851

INTERNATIONAL SEARCH REPORT

International application No.
PCT/AU2006/001397

C (Continuation). DOCUMENTS CONSIDERED TO BE RELEVANT

Category*	Citation of document, with indication, where appropriate, of the relevant passages	Relevant to claim No.
X	US 2005/0068631 A1 (LIU ET AL.) 31 March 2005 See figure 1 and paragraphs [0073] – [0113]	1,5,11,12,14
A	GB 2174198 A (ELF FRANCE) 29 October 1986 See entire document	
A	Derwent Abstract Accession No. A7690A/04, Class R14, FR 2346698 (MARECHAL) 2 December 1977 See abstract	
A	US 6433876 B1 (KUHN) 13 August 2002 See entire document	
A	Derwent Abstract Accession No. 2005-535627/55, Class P31; S02, FR 2865538 A1 (CNRS CENT NAT RECH SCI) 29 July 2005 See abstract	

INTERNATIONAL SEARCH REPORT

Information on patent family members

International application No.
PCT/AU2006/001397

This Annex lists the known "A" publication level patent family members relating to the patent documents cited in the above-mentioned international search report. The Australian Patent Office is in no way liable for these particulars which are merely given for the purpose of information.

Patent Document Cited in Search Report		Patent Family Member					
EP	1519170	US	7016040	US	2005062966		
US	6212313	US	6215923				
US	5135183	NONE					
US	2005068631	CN	1529425	US	7113279		
GB	2174198	DE	3612733	FR	2581190	JP	61250543
		US	4732480				
FR	2346698	NONE					
US	6433876	US	6404544	US	6459490	US	2002089741
FR	2865538	EP	1711776	WO	2005080912		

Due to data integration issues this family listing may not include 10 digit Australian applications filed since May 2001.

END OF ANNEX